Published in final edited form as:

Neurobiol Aging. 2015 February ; 36(2): 886–900. doi:10.1016/j.neurobiolaging.2014.10.034.

Intraneuronal Aβ accumulation induces hippocampal neuron hyperexcitability through A-type K^+ current inhibition mediated by activation of caspases and GSK-3

Federico Scala[a], **Salvatore Fusco**[a], **Cristian Ripoli**[a], **Roberto Piacentini**[a], **Domenica Donatella Li Puma**[a], **Matteo Spinelli**[a], **Fernanda Laezza**[b], **Claudio Grassi**[a,*], and **Marcello D'Ascenzo**[a,*]

[a]Institute of Human Physiology, Medical School, Università Cattolica, Rome, Italy

[b]Department of Pharmacology and Toxicology, University of Texas Medical Branch, Galveston, TX, USA

Abstract

Amyloid β-protein (Aβ) pathologies have been linked to dysfunction of excitability in neurons of the hippocampal circuit, but the molecular mechanisms underlying this process are still poorly understood. Here, we applied whole-cell patch-clamp electrophysiology to primary hippocampal neurons and show that intracellular $A\beta_{42}$ delivery leads to increased spike discharge and action potential broadening through downregulation of A-type K^+ currents. Pharmacologic studies showed that caspases and glycogen synthase kinase 3 (GSK-3) activation are required for these $A\beta_{42}$-induced effects. Extracellular perfusion and subsequent internalization of $A\beta_{42}$ increase spike discharge and promote GSK-3-dependent phosphorylation of the Kv4.2 α-subunit, a molecular determinant of A-type K^+ currents, at Ser-616. In acute hippocampal slices derived from an adult triple-transgenic Alzheimer's mouse model, characterized by endogenous intracellular accumulation of $A\beta_{42}$, CA1 pyramidal neurons exhibit hyperexcitability accompanied by increased phosphorylation of Kv4.2 at Ser-616. Collectively, these data suggest that intraneuronal $A\beta_{42}$ accumulation leads to an intracellular cascade culminating into caspases activation and GSK-3-dependent phosphorylation of Kv4.2 channels. These findings provide new insights into the toxic mechanisms triggered by intracellular $A\beta_{42}$ and offer potentially new therapeutic targets for Alzheimer's disease treatment.

*Corresponding authors at: Institute of Human Physiology, Medical School, Università Cattolica "S. Cuore", Largo Francesco Vito 1, 00168 Rome, Italy. Tel.: +39 0630154966; fax: +39 0630154665. grassi@rm.unicatt.it (C. Grassi), dascenzo@rm.unicatt.it (M. D'Ascenzo). .

Disclosure statement

None of the authors has any actual or potential conflicts of interest to report. All animal procedures were approved by the Ethics Committee of the Catholic University and complied with the Italian Ministry of Health guidelines and with national laws (legislative decree 116/1992) and the European Union guidelines on animal research (No. 86/609/EEC).

Appendix A. Supplementary data

Supplementary data associated with this article can be found, in the online version, at http://dx.doi.org/10.1016/j.neurobiolaging.2014.10.034.

Keywords

Amyloid-β protein; Intrinsic excitability; A-type K^+ current; Caspase; GSK-3; KV4.2; Alzheimer's disease; Hippocampal neurons

1. Introduction

Alzheimer's disease (AD) is the most common form of dementia with a high prevalence among the aging population (Citron, 2010). Extracellular fibrillar amyloid β-protein (Aβ) accumulation and neurofibrillary tangles composed of hyperphosphorylated tau are considered the neuropathologic hallmarks of AD (Selkoe, 2001). Aβ originates from the amyloid β-precursor protein (APP) through sequential cleavage by the β- and the γ-secretase enzyme complex (Thinakaran and Koo, 2008). Most of the full-length Aβ peptide consists of the 40-amino-acid long Aβ ($Aβ_{40}$), whereas a small proportion (10%) is the 42-residues variant ($Aβ_{42}$), a species that because of its high hydrophobicity has been considered more prone to fibril formation and neurotoxicity than the $Aβ_{40}$ (Jarrett et al., 1993).

A plethora of neurophysiological studies have reported toxic activity of $Aβ_{42}$ oligomers on synaptic function and activity-dependent plasticity in the hippocampus and cerebral cortex building the notion that AD is a synaptopathy (Crimins et al., 2013; Klyubin et al., 2012; Selkoe, 2002; Shankar et al., 2008; Sheng et al., 2012). It is believed, indeed, that disruption in synaptic structure and function induced by $Aβ_{42}$ is one of the underlying mechanisms leading to the aberrant neuronal processing and network dysfunction that characterize AD cognitive impairment and memory loss (Mucke and Selkoe, 2012). Surprisingly, although, much less knowledge has been gained on other Aβ toxic effects on neuronal activity that might precede synaptic dysfunction and as such could be targeted for early therapeutic interventions against AD.

Emerging evidence indicates that changes in neuronal excitability could play a fundamental role in initiating early $Aβ_{42}$ pathology predisposing to and/or triggering subsequent synaptic dysfunction. In vitro and animal model studies have demonstrated that Aβ pathology associates with increased excitability of hippocampal neurons, leading to hypersynchronous network activity and higher risk for seizures (Born et al., 2014; Brown et al., 2011; Busche et al., 2012; Davis et al., 2014; Del Vecchio et al., 2004; Minkeviciene et al., 2009; Palop et al., 2007; Putcha et al., 2011). Epidemiologic studies have confirmed comorbidity between patients with AD and epilepsy, showing increased risk of seizures in AD patients (Amatniek et al., 2006; Hommet et al., 2008). This repertoire of cellular and clinical studies indicating potential commonalities in early AD and epilepsy opens new horizons in the understanding of early AD triggers and therapies. However, despite this evidence, the molecular mechanisms linking Aβ pathology to aberrant neuronal firing is still poorly understood. A missing link in associating Aβ effects to neuronal excitability is the identification of the source of toxic oligomers.

Early studies based on the observation of senile plaques in the extracellular space (Hardy and Selkoe, 2002) have pointed for extracellular $Aβ_{42}$ ($eAβ_{42}$) as the primary cause of AD. However, in studies on postmortem AD and mild cognitively impaired patients

immunoreactivity of intracellular $A\beta_{42}$ ($iA\beta_{42}$) has been identified in neurons of the hippocampus and entorhinal cortex (Gouras et al., 2000; Mori et al., 2002), the 2 main brain regions affected in early AD pathology. These findings have been corroborated by results from transgenic mouse models (Guzman et al., 2014; Youmans et al., 2012; for review see; LaFerla et al., 2007), leading to the overall hypothesis of iAβ accumulation as an early triggering event in the AD progression preceding senile plaques (Kuo et al., 2001; LaFerla et al., 2007; Oakley et al., 2006). Intracellular Aβ-driven effects on neuronal firing might therefore be one of the earliest detectable triggers of the AD pathology preceding and predisposing to synaptic deficits.

Building on the growing interest in identifying early Aβ targets, we studied the effect of $iA\beta_{42}$ on neuronal excitability in primary hippocampal neurons and in CA1 hippocampal neurons of triple-transgenic AD (3xTg-AD) mouse model that harbor the mutant genes for amyloid precursor protein (APPSwe), presenilin 1PS1M146V and for tauP301L (Oddo et al., 2003) and overexpresses intracellular $A\beta_{42}$.

We found that $A\beta_{42}$ internalization is required for inducing increase in intrinsic excitability in hippocampal pyramidal neurons, an effect that is mediated by inhibition of A-type K^+ channels (Kv), and requires caspases activation and glycogen synthase kinase 3-(GSK-3) dependent phosphorylation of Kv4.2. Parallel changes in intrinsic excitability, A-type K^+ currents, and Kv4.2 phosphorylation are found in CA1 hippocampal neurons derived from brain slices of 3xTg-AD mice.

2. Methods

2.1. Animals

A colony of 3xTg-AD (harboring the PS1 M146V, APPSwe KM670/671NL, and tau P301L transgenes) and non-transgenic (B6129SF2/J, named non-Tg) mice were used for electrophysiological experiments in brain slices and for Western blot analysis. The colonies were established in-house from breeding pairs purchased by the Jackson Laboratory. All animal procedures were approved by the Ethics Committee of the Università Cattolica “S. Cuore” and were fully compliant with the Italian and European Union legislation on animal research.

2.2. Preparation of $A\beta_{42}$ solutions

Freeze-dried purified $A\beta_{42}$, $A\beta_{42\text{-}1}$, and $A\beta_{42}$ variant harboring oxidized methionine in position 35 ($A\beta_{42}^{MO}$) were purchased from rPeptide (Bogard, GA) and AnaSpec (Fremont, CA). Protein solutions were prepared as previously described (Ripoli et al., 2013), according to standard procedures. Briefly, peptides were diluted to 1 mM in 1,1,1,3,3,3,-hexafluoro-2-propanol to disassemble preformed aggregates and stored as dry films at −20 °C before use. The films were dissolved at 1 mM in dimethyl sulfoxide (DMSO), sonicated for 10 minutes, diluted to 100 μM in cold phosphate-buffered saline (PBS), and incubated for 12 hours at 4 °C to promote protein oligomerization. The final working concentration of 200 nM was obtained by diluting the 100 μM $A\beta_{42}$ in extracellular or intracellular solutions (for salt

concentrations see the following sections). The same amount of DMSO to PBS contained in $A\beta_{42}$ solutions was used as vehicle.

2.3. Primary hippocampal neuron cultures

Hippocampal neurons from postnatal day 0–2, C57Bl/6 mice brains were prepared according to standard procedure (Piacentini et al., 2008) with some modifications. Briefly, hippocampi were incubated for 10 minutes at 37 °C in PBS containing trypsin-ethylenediaminetetraacetic acid (0.025%/0.01% wt/vol; Biochrom AG, Berlin, Germany), and the tissue was mechanically dissociated at room temperature (RT) with a fire-polished Pasteur pipette. The cell suspension was harvested and centrifuged at 235*g* for 8 minutes. The pellet was suspended in 88.8% Minimum Essential Medium (Biochrom), 5% fetal bovine serum, 5% horse serum, 1% glutamine (2 mM), 1% penicillin-streptomycin-neomycin antibiotic mixture (Invitrogen, Carlsbad, CA), and glucose (25 mM). Cells were plated at a density of approximately 100,000 cells on 20-mm coverslips precoated with poly-L-lysine (0.1 mg/mL; Sigma, St. Louis, MO). Twenty-four hours later, the culture medium was replaced with a mixture of 96.5% Neurobasal medium (Invitrogen), 2% B-27 (Invitrogen), 0.5% glutamine (2 mM), and 1% penicillin-streptomycin-neomycin antibiotic mixture. After 72 hours, this medium was replaced with a glutamine-free version of the same medium, and the cells were grown for 10 more days before experiments. The removal of L-glutamine from the culture medium was used to limit the grown of “mitotic” cells, such as astrocytes, and to reduce the possible excitotoxicity induced by glutamate obtained from the enzymatic conversion of L-glutamine.

2.4. Study of Aβ internalization

To study internalization of $A\beta_{42}$, both *wt* and $A\beta_{42}^{MO}$ were labeled with the IRIS 5-NHS active ester dye (IRIS 5; λex: 633 nm; λem: 650–700 nm; Cyanine Technology, Turin, Italy) according as previously described (Ripoli et al., 2013). IRIS-5 dye is suitable for conjugation of any biomolecules carrying free primary amines, such as proteins and peptides. Briefly, Aβ solutions (100 μM in PBS) were mixed with 6 mM IRIS 5 in DMSO for 4 hours in the dark under mild shaking conditions. After this time, labeled Aβs were purified with Vivacon 500 ultrafiltration spin columns (2 KDa cutoff; Sartorius Stedim Biotech GmbH, Goettingen, Germany) and then resuspended in PBS at a concentration of 100 μM before final dilution in the culture medium. Time-dependent internalization IRIS-5-labeled $A\beta_{42}$ (either *wt* or MO) was then studied by immunocytochemistry in hippocampal neurons derived from C57 mice.

Hippocampal neurons cultured for 15 days and treated with IRIS-5-labeled Aβ42 analogs were fixed with 4% paraformaldehyde (Sigma) in PBS for 15 minutes at RT. After being permeabilized (15 minutes incubation with 0.3% Triton X-100 [Sigma] in PBS), cells were incubated for 20 minutes with 0.3% BSA in PBS to block nonspecific-binding sites and then overnight at 4 °C with mouse anti-microtubule–associated protein 2 (MAP2, 1:300; Sigma). The subsequent day, cells were washed twice in PBS and then reincubated for 90 minutes at RT with Alexa-fluor 488-labeled donkey anti-mouse secondary antibody. Images (512 × 512 pixels) were acquired at 63× magnification with a confocal laser scanning system (TCS-SP2, Leica) and an oil-immersion objective (N.A. 1.4). Alexa-fluor 488 and IRIS-5 were excited

at 488 and 633 nm, respectively with Ar/Kr and He/Ne lasers. The fluorescent signals emitted from fluorophores were revealed in spectral windows ranging from 500 to 530 nm for Alexa 488 and from 650 to 700 nm for IRIS-5. DAPI staining was imaged after 2-photon excitation (760 nm) with an ultrafast, tunable, mode-locked titanium:sapphire laser (Chamaleon, Coherent Inc).

2.5. Electrophysiology on primary hippocampal neurons

Recordings were obtained with an Axopatch 200B amplifier (Molecular Devices), and stimulation and data acquisition were performed with the Digidata 1200 series interface and pCLAMP 10 software (Molecular Devices). Patch electrodes, fabricated from borosilicate glass capillaries with the aid of a micropipette puller (P-97, Sutter Instruments, Novato, CA) had resistances of 3–5 MΩ when filled with the internal solution that contained (in mM): 146 mM K-gluconate, 18 mM HEPES, 1 mM EGTA, 4.6 mM $MgCl_2$, 4 mM NaATP, 0.3 mM Na_2GTP, and 15 mM creatine phosphate, (pH 7.4). For recordings, cells were constantly perfused with an external Tyrode solution containing the following (in mM): 140NaCl; 2 KCl; 10 HEPES; 10 glucose; 4 $MgCl_2$; and 4 $CaCl_2$ (pH 7.4; 312 mOsm). Primary neuronal cultures used in our study contained a mixed population of neurons and glial cells. According to previous studies (Bonin et al., 2007), pyramidal neurons were selected based on their pyramidal-like shape soma (approximately 15–20 μm in diameter) with prominent apical dendrites and physiological properties. A few cells (approximately 2%) exhibited large, fast after hyperpolarizations and higher discharge rates than those of most cells—features that are typical of fast-spiking GABAergic interneurons— and they were excluded from further investigation. We monitored the access resistance and membrane capacity before and at the end of the experiments to ensure recording stability and the health of studied cells (Grassi et al., 2004). Recordings were considered stable when the series and input resistances, resting-membrane potential, and stimulus artifact duration did not change >20%. To measure spike firing, current pulses (800 ms duration, from −50 to 250 pA) were applied in current-clamp mode. Depolarizing current pulses were applied every 5 minutes. Membrane potentials were held at approximately −70 mV during interpulse interval by passage of direct current with the patch amplifier. Changes in firing after 20 minutes of exposure to intracellular or extracellular $A\beta_{42}$ given compound were determined as the percent change in number of action potentials (APs) generated relative to baseline (T = 0). For eliciting single spikes, brief depolarization currents (1 nA; 2 ms) were injected. Spike halfwidth was measured at 50% of the peak. The transient A-type K^+ current involtage–clamp mode was recorded by applying 300 ms voltage step from −90 to +50 mV. The transient channel was inactivated for a voltage step from −30 to +50 mV, leaving the sustained current of the total outward current. The transient current was then isolated by a digital subtraction of the sustained current from the total outward current.

2.6. Slices preparation and electrophysiology

Coronal slices (300- to 400-μm thick) containing the hippocampi were prepared using standard procedures (Podda et al., 2004, 2008; Curcio et al., 2013). Briefly, the animals were anesthetized with halothane (Sigma) and decapitated. The brains were rapidly removed and placed in ice-cold cutting solution containing in mM: 124 NaCl, 3.2 KCl,1 NaH_2PO_4, 26 $NaHCO_3$, 2 $MgCl_2$, 1 $CaCl_2$, 10 glucose, 2 Na-pyruvate, and 0.6 ascorbic acid (pH 7.4,

95%O_2/5% CO_2). Slices were cut with a vibratome (VT1000 S, Leica Microsystems, Wetzlar, Germany) and incubated in the cutting solution at 32 °C for at least 1 hour and then at RT until use. Slices were then transferred to a submerged recording chamber and continuously perfused with artificial cerebrospinal fluid bubbled with 95% O_2 and 5% CO_2 (pH 7.4). The artificial cerebrospinal fluid contained (in mM): 124 NaCl, 3.2 KCl, 1 NaH_2PO_4, 26 $NaHCO_3$, 1 $MgCl_2$, 2 $CaCl_2$, 10 glucose. The flow rate was kept at 1.5 mL/min with a peristaltic pump (Minipuls 3, Gilson), and bath temperature was maintained at 30 °C–32 °C by an inline solution heater and temperature controller (TC-344B, Warner Instruments, Hamden, CT, USA). Hippocampal pyramidal neurons were identified with a ×40 water-immersion objective on an upright microscope equipped with differential interface contrast optics under infrared illumination (BX5IWI, Olympus) and video observation. Current-clamp recordings were made with a MultiClamp 700B amplifier (Molecular Devices). Whole-cell patch-clamp recordings were performed with pipettes (resistance of 3–5 MΩ) filled with internal solution containing (in mM): 145 K-gluconate, 2 $MgCl_2$, 0.1 EGTA, 2 Na_2ATP, and 10 HEPES (pH 7.2 with KOH; 290 mOsm). Access resistance was monitored throughout the recording and was typically <15 MΩ. Data acquisition and stimulation were performed with a Digidata 1440A Series interface and pClamp 10 software (Molecular Device). Data were filtered at 1 kHz, digitized at 10 kHz, and were analyzed off-line with pClamp 10 software. To measure firing, current pulses were applied using a patch amplifier in current-clamp mode. A series of 5–6 depolarizing current pulses (800 ms duration, 50 pA apart) were applied (D'Ascenzo et al., 2009). Membrane potentials were held at approximately −70 mV during inter-pulse intervals by injecting Direct current with the patch-clamp amplifier. For eliciting single spikes, brief depolarization currents (1 nA; 2 ms) were injected. Spike halfwidth was measured at 50% of the peak. In some experiments membrane input resistance was evaluated in current-clamp mode using series of 600 ms hyperpolarizing steps (from −60 to 0 pA in 20 pA increments). Input resistance was calculated from the peak voltage achieved at each step. The input resistance values were derived from the linear portion of the intensity-to-voltage (I–V) relationship as the slope of the linear regression fitting line calculated by using the Clampfit program (pCLAMP9 software, Molecular Devices).

2.7. Immunoblot analysis

For protein expression and phosphorylation, cells or tissues were lysed in ice-cold lysis buffer (NaCl 150 mM, Tris-HCl 50 mM pH 8, EDTA 2 mM) containing 1% Triton X-100, 0.1% SDS, ×1 protease inhibitor mixture (Sigma), 1 mM sodium orthovanadate, and 1 mM sodium fluoride (Podda et al., 2012). After 15 minutes on ice with occasional vortexing, cells were spun down at 22,000*g*, 4 °C to remove debris, and supernatant quantified for protein content (DC Protein Assay; Bio-Rad). Equal amounts of cell protein lysates were diluted in 6× Laemmli buffer, boiled and resolved by SDS-PAGE.

Western blotting was performed using primary antibodies 1:1000 diluted overnight and revealed with horseradish peroxidase-conjugated secondary antibodies diluted to 1:2000 (Cell Signaling). The following primary antibodies were used: anti-total Kv4.2 rabbit polyclonal antibody from Abcam, anti-pKv4.2 phosho-Ser-616 rabbit polyclonal antibody from MyBioSource, anti-total GSK-3β rabbit monoclonal antibody from Cell Signaling,

anti-GSK-3β phosho-Ser-9 rabbit polyclonal antibody from Immunological Sciences, and anti-tubulin mouse monoclonal antibody from Sigma.

For analysis of $A\beta_{42}$ peptide protein, preparations were analyzed by Western blotting as previously described (Attar et al., 2012; Ripoli et al., 2013). Briefly, the Aβ samples were mixed with NuPAGE LDS sample buffer 4× (final concentration of 200 nM) and separated on 10%–20% gradient Novex Tricine precast gels (Invitrogen) according to the manufacturer's protocol. After electrophoresis the proteins were transferred to 0.2-μm nitrocellulose membranes (Amersham Biosciences, Buckinghamshire, UK). Membranes were blocked for 1 hour, at RT, in a suspension of 5% non-fat milk in Tris-buffered saline containing 0.1% Tween-20 before incubation overnight at 4 °C with mAb 6E10 (Signet, Dedham, MA, USA; 1:1000). Membranes were washed 3 times with Tris-buffered saline containing 0.1% Tween-20 and then incubated with horseradish peroxidase-conjugated anti-mouse secondary antibody (Cell Signaling; 1:2000) at RT for 1 hour. Development was done after 5 minutes of incubation with enhanced chemiluminescence reagents (Super-Signal west Femto Pierce) and exposed to Hyperfilm (Amersham Biosciences). Molecular sizes for immunoblot analysis were determined using color marker ultra-low range (Sigma).

2.8. Statistical analysis

Data are expressed as means ± standard errors of the means. Statistical significance was assessed with either Student t test or paired t test and 1-way analysis of variance for multiple groups comparison (with Tukey post hoc test). Statistical analysis was performed with SYSTAT 10.2 software (Statcom, Inc, Richmond, CA). The level of significance was set at 0.05.

3. Results

3.1. Intracellular $A\beta_{42}$ increases neuronal firing in primary mouse hippocampal neurons

To investigate whether $iA\beta_{42}$ affects intrinsic excitability, whole-cell patch-clamp recordings were performed on primary mouse hippocampal neurons in current-clamp mode. Action potential firing was examined by exposing cells to a series of 800 ms current pulses (1 every 5 minutes), whereas recombinant $A\beta_{42}$ (200 nM) was intracellularly perfused through the patch pipette. The amplitude of current pulses ranged from −50 pA (hyperpolarizing, sub-threshold) to 200 pA (depolarizing, suprathreshold) in 50 pA increments. After 20 minutes (T_{20}) of $A\beta_{42}$ perfusion, the number of spikes significantly increased compared with the beginning of the experiment, right after achieving whole-cell configuration (T_0) (Fig. 1A, C, and D; number of APs at T_0 was 8.7 ± 0.6 versus 12.4 ± 0.8 at T_{20}; n = 22; $p < 0.001$; paired *t* test). The $A\beta_{42}$-induced firing enhancement developed quite slowly and peaked approximately 10 minutes after intracellular application of $A\beta_{42}$ (Fig. 1C, black circles). Similar effects were also found at a more physiological temperature (36 °C; Supplementary Fig. 1). To rule out nonspecific effects of $A\beta_{42}$ either the vehicle or 200 nM of the reverse protein $A\beta_{42\text{-}1}$ were injected into cells and firing frequency examined. As shown in Fig. 1B–D, neither vehicle nor $A\beta_{42\text{-}1}$ significantly affected spike number (vehicle, number of APs at T_0 8.8 ± 1.0; number of APs at T_{20} = 9.1 ± 1.1, n = 10, $p > 0.05$, paired *t* test; $A\beta_{42\text{-}1}$, number of APs at T_0 = 8.3 ± 1.6; number of APs at T_{20} = 8.4 ± 1.3, n =

7, $p > 0.05$, paired *t* test). The oligomer distribution profile of recombinant $A\beta_{42}$ used in the previously mentioned experiments was verified by Western blot analysis, which showed that the vast majority of the injected $A\beta_{42}$ was in the form of monomers, dimers, trimers, and tetramers (Fig. 1F), that are considered the most synaptotoxic species in AD (Mucke and Selkoe, 2012; Shankar et al., 2008).

A set of dedicated experiments was performed to determine whether $iA\beta_{42}$ affected membrane properties. We found that $iA\beta_{42}$ had no effects on the resting membrane potential ($T_0 = -70.0 \pm 0.3$ mV; $T_{20} = -72.4 \pm 1.2$ mV; n = 5; $p > 0.05$) or cell input resistance ($T_0 = 265.5 \pm 17.8$ MΩ; $T_{20} = 272.7 \pm 14.9$ MΩ; n = 22; $p > 0.05$; paired *t* test).

Importantly $iA\beta_{42}$, but not the vehicle and the reverse peptide $A\beta_{42\text{-}1}$, induced a modest but significant decrease in the first spike latency (Fig. 1E; $iA\beta_{42}$: $T_0 = 49.8 \pm 13.2$ ms; $T_{20} = 31.8 \pm 6.7$ ms; n = 22; $p < 0.05$; paired *t* test; vehicle: $T_0 = 48.4 \pm 10.3$ ms; $T_{20} = 46.9 \pm 8.7$ ms; n = 10; $p > 0.05$; paired t test; $A\beta_{42\text{-}1}$: T0 = 49.1 ± 8.8 ms; $T_{20} = 51.5 \pm 9.5$ ms; n = 7; $p > 0.05$; paired t test). A concomitant change in spike width was found in an additional set of experiments in which the AP shape was analyzed with a series of single depolarizing steps (1 nA; 2 ms, Fig. 1G). As shown in Fig. 1H, 20 minutes of $iA\beta_{42}$ perfusion, but not vehicle and $iA\beta_{42\text{-}1}$, significantly broadened the AP ($iA\beta_{42}$: $T_0 = 1.9 \pm 0.2$ ms; $T_{20} = 2.5 \pm 0.3$ ms; n = 10; $p < 0.001$; paired *t* test; $iA\beta_{42\text{-}1}$: $T_0 = 1.8 \pm 0.2$ ms; $T_{20} = 1.7 \pm 0.1$ ms; n = 7; $p > 0.05$; paired *t* test; vehicle: $T_0 = 2.1 \pm 0.2$ ms; $T_{20} = 2.2 \pm 0.1$ ms; n = 7; $p > 0.05$; paired *t* test). Broadening of APs was also observed in the first AP in a train of spikes evoked by 800 ms depolarizing pulse ($T_0 = 1.7 \pm 01$ ms; $T_{20} = 2.3 \pm 0.2$ ms; n = 22; $p < 0.001$). Reduced first spike latency and broadening of the spike width are consistent with a decrease in A-type K^+ currents (Kim et al., 2005; McDermott and Schrader, 2011). The A-type K^+ current is a voltage-dependent, transient, and outward current that has been shown to control action potential repolarization in hippocampal neurons (Carrasquillo et al., 2012; Kim et al., 2005). Taken together, these results suggest that intracellular accumulation of $A\beta_{42}$ increases intrinsic neuronal excitability, likely through an A-type K^+ current-mediated mechanism.

We therefore hypothesized that the increased excitability induced by iAβ perfusion could be due, at least in part, to a downregulation of A-type K^+ current. To test this hypothesis, we evaluated the magnitude of A-type K^+ currents during intracellular perfusion of $A\beta_{42}$ or vehicle in voltage-clamp mode. Representative traces of the total outward current recorded in response to voltage steps from −90 to +50 mV are shown in Fig. 2A (upper trace). A prepulse of −30 mV (50 ms) was applied to inactivate A-type K^+ transient currents and to isolate the sustained current component (Fig. 2A, middle trace; Hoffman and Johnston, 1998). The transient current was subsequently obtained by digital subtraction (total sustained, Fig. 2A, lower trace). When K^+ currents were recorded in the presence of 5 mM 4-AP, a commonly used A-type K^+ current blocker, the currents were strongly inhibited thus confirming the A-Type identity of the K^+ currents (Fig. 2B). As shown in Fig. 2C, intracellular $A\beta_{42}$ infusion, but not vehicle and $A\beta_{42\text{-}1}$, significantly decreased A-type K^+ currents with a time course similar to $iA\beta_{42}$-induced increase in spike number (Fig. 2C–E; $A\beta_{42}$: T_0 1916 ± 292 pA; $T_{20} = 1141 \pm 196$ pA; n = 11; $p < 0.001$; paired *t* test; vehicle: $T_0 = 1866 \pm 256$ pA; $T_{20} = 1881 \pm 232$ pA; n = 10; $p > 0.05$; $A\beta_{42\text{-}1}$: $T_0 = 1884 \pm 297$ pA; $T_{20} = 1836 \pm 145$ pA; n = 6; $p > 0.05$). These results demonstrate that intracellular accumulation

of $A\beta_{42}$ increases intrinsic excitability in hippocampal neurons and suggest that this effect may be because of reduction of A-type K^+ current.

To provide additional evidence for the involvement of A-type K^+ current in the $iA\beta_{42}$-induced neuronal hyperexcitability, we performed a set of experiments in which we added 60 μM of 4-AP to the bath solution before achievement of the whole-cell configuration. At this concentration, 4-AP reduces the A-type K^+ current (approximately 30%) to a level that still allows the cell to fire (Mitterdorfer and Bean, 2002; Ye et al., 2003). Under these conditions, $iA\beta_{42}$ had no effect on neuronal excitability (Fig. 1D; number of APs at T_0 = 12.0 ± 1.1; number of APs at T_{20} = 11.4 ± 0.7; n = 7; $p > 0.05$; paired *t* test), thus supporting our hypothesis that $A\beta_{42}$-induced reduction of A-type K^+ current leads to increased intrinsic excitability.

3.2. $iA\beta_{42}$-induced increased excitability and A-type K^+ current reduction require caspase and GSK-3 activation

Our next objective was to identify intracellular pathways that mediate the observed $iA\beta_{42}$-induced hyperexcitability.

Caspases, key molecular proteases involved in apoptosis (Nicholson, 1999) have been implicated in hippocampal synaptic plasticity (Jo et al., 2011; Li and Sheng, 2012), have been associated with AD and can be activated on Aβ exposure (Allen et al., 2001; Cho and Johnson, 2004; Chong et al., 2006; Heneka et al., 2013; Jo et al., 2011; Mattson, 2004).

To determine whether caspases might be involved in the $iA\beta_{42}$-induced increase in intrinsic excitability, we tested whether Z-VAD-FMK, a pan-caspase inhibitor (Li and Sheng, 2012) could prevent $iA\beta_{42}$-induced hyperexcitability. When $A\beta_{42}$ was intracellularly perfused in hippocampal neurons that were preincubated (20 minutes) with 50 μM of Z-VAD-FMK, no changes in excitability were detected (Fig. 3A and B; number of APs at T_0 = 8.0 ± 1.2; number of APs at T_{20} = 7.5 ± 0.8; n = 10; $p > 0.05$; paired *t* test). Likewise, A-type K^+ currents and AP width were unaffected by the $A\beta_{42}$ treatment (for A-type K^+ currents Fig. 3C–E, T_0 = 1932 ± 164 pA; T_{20} = 1783 ± 174 pA; n = 8; $p > 0.05$; for AP width, Fig. 3F–G; halfwidth at T_0 = 1.94 ± 0.08; halfwidth at T_{20} = 2.01 ± 0.05; n = 8; $p > 0.05$; paired *t* test). Of note, exposure of neurons, treated with vehicle, to Z-VAD-FMK had no effects on spike number (Fig. 3B; number of APs at T_0 = 9.3 ± 0.9; number of APs at $T2_0$ = 8.7 ± 0.7; n = 10; $p > 0.05$; paired *t* test).

The results demonstrate that inhibition of caspases occludes the effect of $iA\beta_{42}$ on excitability and strongly suggest that caspases are a downstream target of $iA\beta_{42}$.

Another protein that has been widely implicated in AD is GSK-3β (Medina and Avila, 2013; Phiel et al., 2003; Takashima, 2006). GSK-3β activity is normally suppressed by its N-terminal phosphorylation at Ser-9 induced by protein kinase type 1 (Akt-1) (Emamian et al., 2004; Jo et al., 2011). Caspase-3 activation cleaves Akt1 resulting in derepression and increased activity of GSK-3β (Deng et al., 2014; Jo et al., 2011). Upregulation of GSK-3β interferes with synaptic plasticity mechanisms (Bradley et al., 2012) and voltage-gated Na^+, Ca^{2+}, and K^+ channel function (Wildburger and Laezza. 2012).

We, therefore, speculated that $A\beta_{42}$-induced neuronal hyperexcitability could be mediated by GSK-3 activation, as a downstream of caspase-3. In support of this hypothesis, we found that pre-incubation (20 minutes) of the hippocampal neurons with the specific GSK-3 inhibitor CT-99021 (1 μM) prevented $iA\beta_{42}$-induced spike discharge increase (Fig. 4A and B; APs at $T_0 = 6.4 \pm 1.9$; APs at $T_{20} = 7.4 \pm 2.6$; n = 7; $p > 0.05$; paired *t* test), AP width increase (Fig. 4F and G; halfwidth at $T_0 = 1.97 \pm 0.24$; halfwidth at $T_{20} = 2.16 \pm 0.28$; n = 11; $p > 0.05$; paired *t* test) and A-type K^+ current reduction (Fig. 4C–E; $T_0 = 1900 \pm 379$ pA; $T_{20} = 1719 \pm 344$ pA; n = 7; $p > 0.05$). These results strongly suggest that the $iA\beta_{42}$-induced increase in intrinsic excitability requires the activity of the GSK-3 pathway.

3.3. Intracellular $A\beta_{42}$ accumulation is required for the extracellular Aβ-induced increase in intrinsic excitability

We next asked whether eAβ could mimic the effects of $iA\beta_{42}$ and act through similar mechanisms. As shown in Fig. 5, $eA\beta_{42}$ oligomers (200 nM) significantly increased the number of spikes evoked in response to current steps (Fig. 5A–C; APs at $T_0 = 8.5 \pm 0.9$; APs at $T_{20} = 12.7 \pm 1.5$; n = 7; $p < 0.05$; paired *t* test). The magnitude of the phenotype was comparable with $iA\beta_{42}$ although the time course of the effect was slightly slower (Fig. 5B, solid circles). Similarly to $iA\beta_{42}$, $eA\beta_{42}$ affected spike kinetics (halfwidth: $T_0 = 1.8 \pm 0.1$; $T_{20} = 2.1 \pm 0.1$; n = 7; $p < 0.05$; first spike latency: $T_0 = 48.9 \pm 12.0$; $T_{20} = 27.8 \pm 11.2$; n = 7; $p < 0.05$) and reduced the amplitude of A-type K^+ currents (Supplementary Fig. 1; $T_0 = 1988 \pm 375$ pA; $T_{20} = 1232 \pm 295$ pA; n = 6; $p < 0.05$; paired *t* test), a phenotype that was prevented by preincubation of neurons with either Z-VAD-FMK (Fig. 5C; APs at $T_0 = 9.6 \pm 0.8$; APs at $T_{20} = 8.5 \pm 1.1$; n = 8; $p > 0.05$; paired *t* test) or CT-99021 (Fig. 5C; APs $T_0 = 9.2 \pm 1.8$; APs $T_{20} = 8.5 \pm 2.4$; n = 7; $p > 0.05$; paired *t* test). These results suggest that $eA\beta_{42}$ and $iA\beta_{42}$ share common mechanisms of action and signal transduction.

To gain further mechanistic insights into the $eA\beta_{42}$ activity, total cell lysates obtained from hippocampal neurons treated with $eA\beta_{42}$ were processed for Western blot analysis and probed for a GSK-3β Ser-9 antibody, commonly used to estimate the pool of active GSK-3 (Fig. 5D). Band quantification revealed a time-dependent decrease of active GSK-3 induced by $eA\beta_{42}$, whereas the total GSK-3 pool remained constant (Fig. 5E). Furthermore, preincubation of hippocampal neurons with the caspase inhibitor ZVAD-FMK (50 μM; 20 minutes) prevented the $eA\beta_{42}$-induced decrease in GSK-3 phosphorylation, suggesting that GSK-3 is a downstream target of $A\beta_{42}$ via caspases 3 activation (Supplementary Fig. 3). Thus, by decreasing the level of tonic GSK-3 inhibition $eA\beta_{42}$ might markedly increase the GSK-3 active pool with consequences for neuronal excitability (Kapfhamer et al., 2010; Wildburger and Laezza, 2012).

Overall, these results demonstrate that exposure of neurons to either $eA\beta_{42}$ or $iA\beta_{42}$ (by intracellular perfusion) leads to a common pathophysiological outcome on excitability raising the question of whether $eA\beta_{42}$ requires internalization for its toxic activity. Two different approaches were used to answer this question.

First, we sought to determine whether extracellular perfusion of a cell membrane impermeable form of $A\beta_{42}$ harboring the methionine 35 sulfoxide chemical modification

($A\beta_{42}^{MO}$) (Ripoli et al., 2013), retained $A\beta_{42}$ activity. As shown in Fig. 6A, $A\beta_{42}^{MO}$ had no effect on neuronal excitability if bath applied (APs at T_0 = 9.4 ± 0.8; APs at T_{20} = 9.5 ± 1.3; n = 7; $p > 0.05$; paired *t* test) but was significantly active if injected intracellularly (Fig. 6A; APs T_0 = 9.0 ± 1.3; APs T_{20} = 12.7 ±1.8; n = 7; $p < 0.05$; paired *t* test). These results indicate that the lack of effect of bath applied $A\beta_{42}^{MO}$ can be attributed to impaired internalization rather than disrupted intracellular activity. Furthermore, to provide evidence for lack of $A\beta_{42}^{MO}$ internalization, we conjugated Aβ42 wild type ($A\beta_{42}^{WT}$) and $A\beta_{42}^{MO}$ with the fluorescent dye IRIS-5-NHS and examined the cellular distribution of the 2 $A\beta_{42}$ variants with confocal microscopy. Results of this set of experiment showed that more than 90% of neurons treated for 30 minutes with IRIS-5-labeled $A\beta_{42}^{WT}$ exhibited intracellular accumulation of the peptide (mean number of fluorescent spots for single neuron was 13 ± 3), although no internalization was observed on treatment with IRIS-5-labeled $A\beta_{42}^{MO}$ analog (Fig. 6C). Taken together these results suggest that the $A\beta_{42}$-induced increase of intrinsic excitability likely requires its intracellular accumulation.

Second, we conducted a set of experiments aimed at preventing the activity of $iA\beta_{42}$ with the 6E10 antibody that recognizes human $A\beta_{42}$, but has no reported effects on endogenous $A\beta_{42}$ or APP fragments (Tampellini et al., 2007). As shown in Fig. 6B, intracellular perfusion of the 6E10 antibodyalone (1:300) had no effect on intrinsic excitability (APs at T_0=8.8±1.3; APs at T_{20}=8.4±1.3; n=7; p>0.05; paired *t* test), but significantly lowered the increase in firing induced by $eA\beta_{42}$ (+16.9%±7.9% n=10 compared with +47.0%±9.1%; n=7; $p < 0.005$; unpaired *t* test). Thus, the increase in intrinsic excitability induced by eAβ42 requires its intracellular action.

3.4. $A\beta_{42}$ increases α-subunit Kv4.2 phosphorylation

Our data indicate that intracellular accumulation of $A\beta_{42}$ increases intrinsic excitability in hippocampal neurons through inhibition of A-type K^+ currents via caspases and GSK-3 activation. The molecular determinants of 4-AP-sensitive A-type K^+ currents vary depending on brain regions. The Kv4.2 subunit is prominently expressed in CA1 hippocampal neurons, where it has been proposed to mediate sub-threshold and fast inactivating A-type K^+ currents (Coetzee et al., 1999; Kim and Hoffman, 2012; Lin et al., 2011; Varga et al., 2000). Previous studies showed that Kv4.2 can be phosphorylated by extracellular signal-regulated kinases at Ser-616 resulting in suppression of the channel activity (Hu et al., 2006), indicating that phosphorylation of Kv4.2 can lead to functional outcomes on K^+ currents.

Inspection of the primary sequence of Kv4.2 indicates that Ser-616 lies in a putative GSK-3 phosphorylation motif (S/TXXXS/T;Fig. 7A), where the target site is flanked by a proline residue (P617) and is 3 residues upstream of another S residue (S-620) that usually acts as a phosphorylation priming site (Wildburger and Laezza, 2012). Thus, we hypothesized that $A\beta_{42}$ treatment could result in a GSK-3-dependent phosphorylation of the Kv4.2 subunit at Ser-616.

To test this hypothesis, we preincubated hippocampal neurons with $A\beta_{42}$ (200 nM; 20 minutes) in the presence or absence of CT-99021 (1 μM; 30 minutes) and used Western blot

analysis of total cell lysates to examine the level of phosphorylation of Ser-616. As illustrated in Fig. 7B and C, the $A\beta_{42}$ treatment led to a significant increase ($p < 0.05$; n = 3) in Ser-616 immunoreactivity that was prevented by CT-99021 ($p > 0.05$; n = 3). These results suggest that phosphorylation of Kv4.2 by GSK-3 might be a downstream target of $A\beta_{42}$-mediated increase in intrinsic excitability in hippocampal neurons.

3.5. Intracellular Aβ accumulation in an AD mouse model recapitulates in cell studies

The 3xTg-AD mouse model harbors the mutant genes for APPSwe, presenilin 1PS1M146V and tauP301L (Oddo et al., 2003) and exhibits temporal- and region-specific Aβ and tau pathologies that closely resemble the human AD pathology. At early AD stages (3–5 months), 3xTg-AD mice show intracellular accumulation of Aβ that precedes extracellular plaques (Oddo et al., 2003). As such, 3xTg-AD mice are an ideal model to examine early toxic effects of intracellular $A\beta_{42}$. To determine whether intracellular Aβ accumulation in 3xTg-AD mice recapitulated ours in cell studies, we performed whole-cell patch-clamp recordings of CA1 pyramidal neurons in hippocampal slices obtained from 5-month-old 3xTg-AD and non-Tg mice. Visually identified CA1 pyramidal neurons were exposed to a series of 800 ms current pulses ranging from −50 pA to 200 pA in 50 pA increments. To control for possible effects of membrane depolarization on neuronal firing, the membrane potential was kept at approximately −70 mV by injecting hyperpolarizing current during step intervals. Under these experimental conditions, we observed a significant increase in firing in 3xTg-AD neurons compared with control in almost all ranges of stimulation (Fig. 8A and B). The average AP number at 150 pA current injection was significantly higher in 3xTg-AD mice (16.4 ± 2.1, n = 10; $p < 0.05$ unpaired *t* test) compared with non-Tg (9.1 ± 1.9; n = 10). We also found a significant increase in the AP halfwidth in 3xTg-AD neurons (1.15 ± 0.09, n = 10; $p < 0.05$, unpaired *t* test) compared with non-Tg neurons (0.83 ± 0.02, n = 10). To determine whether these phenotypes were GSK-3-dependent, we performed a set of experiments in which hippocampal slices from 3xTg-AD mice were preincubated with CT-99021 (30±40 minutes; 1 μM). Under these experimental conditions, the averages of AP number and AP halfwidth were similar to those observed in slices from non-Tg mice (Fig. 8B and D; AP number = 10.9 ± 1.3 AP halfwidth = 0.85 ± 0.04; n = 10; $p > 0.05$). Of note, the increased excitability found in CA1 pyramidal neurons of 3x-Tg-AD mice was not associated with changes in input resistance (3xTg-AD: 189.1 ±13.6MΩ, n = 10; non-Tg: 165.2 ± 8.8 MΩ, n = 10; $p > 0.05$; unpaired *t* test) and membrane resting potential (3xTg-AD: −65.5 ±1.62 mV, n = 10; non-Tg: 60.2 ± 2.9 mV, n = 10, $p > 0.05$, unpaired *t* test). Furthermore, the same changes in intrinsic excitability induced by intracellular $A\beta_{42}$ accumulation were observed in control non-Tg mice following $A\beta_{42}$ intracellular injection through the patch pipette (Supplementary Fig. 4).

Notably, Western blot analysis of hippocampal total cell lysates revealed that the levels of Ser-616 phosphorylation of the Kv4.2 subunit were dramatically higher in 3xTg-AD mice compared with control (n = 8; $p < 0.001$), whereas no changes in the total pool of Kv4.2 were observed (Fig. 8E). Altogether, these results confirm our primary culture studies and indicate that increased intrinsic excitability in CA1 hippocampal neurons is an early functional outcome of AD pathology induced by intracellular Aβ.

4. Discussion

The present study revealed that intracellularly injected $A\beta_{42}$ downregulates A-type K^+ currents and increases spike width of hippocampal pyramidal neurons, thereby increasing excitability. These effects require caspases and GSK-3 activation and correlate with an increase in phosphorylation of a molecular determinant of A-type K^+ currents, the Kv4.2 subunit, at Ser-616, a predicted GSK-3 site. At an early AD stage (5 months old), the 3xTg-AD mouse model exhibits intracellular accumulation of Aβ that precedes the appearance of extracellular plaques. In agreement with our findings in cell studies, we found that excitability of CA1 hippocampal neurons is increased in 3xTg-AD mice compared with controls along with phosphorylation of the Kv4.2 subunit at Ser-616. Converging evidence highlights a critical role of iAβ in AD pathology (Gouras et al., 2012; Ripoli et al., 2014; Takahashi et al., 2014; Zepa et al., 2011) and in its symptoms (Steinerman et al., 2008). Our findings provide new important insights into the mechanism of action of iAβ in AD and argue for a toxic effect of iAβ in early stages of the disease.

Previous studies have shown that extracellular Aβ can affect A-type K^+ currents in hippocampal pyramidal neurons (Chen, 2005; Good and Murphy, 1996). However, the mechanism underlying these changes is poorly understood and whether these effects on A-type K^+ currents require Aβ internalization is not known.

In this study, we show that extracellular Aβ application increases intrinsic excitability of hippocampal neurons and downregulates A-type K^+ currents to the same extent of intracellular Aβ. Importantly, we show that this effect required intracellular Aβ buildup. Our electrophysiological data demonstrate a lack of effect of bath applied $A\beta_{42}^{MO}$, an Aβ variant that exhibited reduced internalization in hippocampal neurons (Fig. 6; Ripoli et al., 2013, 2014). Importantly, $eA\beta_{42}^{MO}$ does not activate caspase-3, preventing the sequel of caspase-induced effects on apoptosis (Clementi et al., 2006) and lacks toxic effects on synaptic function (Ripoli et al., 2013). Our immunofluorescence studies demonstrated the inability of $A\beta_{42}^{MO}$ to accumulate intracellularly and showed that $A\beta_{42}^{MO}$ perfused intracellularly retained the activity of the $iA\beta_{42}^{WT}$ (Fig. 5). Furthermore, chelation of $eA\beta_{42}$, achieved by patch-pipette injection of the 6E10 antibody, reduced the effect on excitability. The monoclonal antibody 6E10 recognizes the N-terminus of human $A\beta_{42}$, and efficiently immunoprecipitates oligomeric and monomeric $A\beta_{42}$ present in conditioned medium (Tampellini et al., 2007). In our experimental conditions, 6E10 antibody did not completely abolished the $eA\beta_{42}$,-induced hyperexcitability (Fig. 6C). This may reflect the inability of 6E10 antibody to neutralize all internalized $A\beta_{42}$ in agreement with previous studies (Klyubin et al., 2005; Tampellini et al., 2007).

Extracellular Aβ can bind to several cell surface receptors including LPR, RAGE, FPRL1, NMDA, and α-7AChRs (LaFerla et al., 2007; Penke et al., 2012), and the resulting receptor-Aβ complex can be then internalized into early endosomes (LaFerla et al., 2007). Furthermore, the soluble $A\beta_{42}$ complex associated with apolipoprotein E promotes Aβ internalization (Gylys et al., 2003; Kim et al., 2009; Kuszczyk et al., 2013). Thus, even at later stages of the disease when the predominant form of Aβ is extracellular, the intracellular

pool of Aβ might be replenished and kept at a constant level by e$A\beta_{42}$ reuptake. Based on these observations, it is tempting to speculate that in the human AD pathology $A\beta_{42}$ may exert complex effects on neuronal excitability through a mixed pool of extracellular and intracellular $A\beta_{42}$.

Intracellular $A\beta_{42}$ has been shown to suppress BK channels in pyramidal neurons located in the layer II/III of the rat visual cortex (Yamamoto et al., 2011). In hippocampal neurons, however, $A\beta_{42}$ reduces A-type K^+ currents (Chen, 2005; Good and Murphy, 1996, Fig. 2), suggesting brain area specific effects of $A\beta_{42}$ on excitability. Our observation that 4-AP occludes the effect of i$A\beta_{42}$ on A-type K^+ currents (Fig. 2) rules out a significant role of BK channels and supports the notion that $A\beta_{42}$-induced A-type K^+ current hypofunction represents the primary mechanism underlying increased neuronal excitability in the hippocampus in the Aβ pathology. Other mechanisms, however, should also be considered. Noteworthy are the results from a recent study demonstrating a role of α-7n-AChR in neuronal hyperexcitability following long-term exposure (7 days) to fibrillar $A\beta_{42}$ (Liu et al., 2013). The precise molecular mechanisms of these effects, however, are still unknown.

We show that $A\beta_{42}$-induced increase in excitability depends on caspases and GSK-3 activation. Caspases are a class of proteases instrumental for many cellular functions including cell differentiation, remodeling, and death. Recently, the role caspase-3, specifically, has been identified in nonapoptotic processes in the central nervous system, such as synaptic plasticity, spine structure, and memory formation (D'Amelio and Rossini, 2012; Snigdha et al., 2012).

Emerging evidence associates caspases with AD. Increased immunoreactivity for caspase-3 has been observed in postsynaptic compartments of postmortem brains from early AD patients (Louneva et al., 2008; Sultana et al., 2010). Caspase-3 can be activated by $A\beta_{42}$ exposure (Allen et al., 2001) and can exacerbate Aβ pathology (for review see Rohn, 2010). In a seminal work from Jo et al., 2011 the pan anti-caspases inhibitor, Z-VAD-FMK, was shown to prevent inhibition of LTP induced by $A\beta_{42}$ in CA1 hippocampal neurons, a finding supported by the lack of the $A\beta_{42}$ effect on CA1 LTP in caspase-3 knockout mice. A conclusion from these studies was that caspase-3 mediates Aβ inhibition of LTP by inducing cleavage of Akt1, a negative suppressor of GSK-3, and subsequent increase in the pool of active GSK-3β, detected as a decrease in the levels of p-GSK-3 (Ser-9). Pharmacologic inhibition of GSK-3 prevented the Aβ-induced inhibition of LTP, suggesting an Aβ-induced mechanism in which activation of casapse-3 leads to cleavage of Akt1 and loss of tonic inhibition of GSK-3 (Jo et al., 2011). Our findings showing that pharmacologic inhibition of either caspases (by Z-VAD-FMK) or GSK-3 (by CT-99021) prevented $A\beta_{42}$-induced hyperexcitability (Figs. 3–4) are consistent with the model described by Jo et al. (2011) and further emphasize the role of caspases signaling in nonapoptotic pathways in AD.

GSK-3 is a multifunctional kinase that modulates many fundamental cell processes including cell proliferation and differentiation (Frame and Cohen, 2001), cell survival (Takashima et al., 1993), cell motility (Lucas et al., 1998), and memory formation (Bradley et al., 2012). Hyperphosphorylation of tau and Aβ production in AD have been linked to GSK-3 dysfunction (DaRocha-Souto et al., 2012; Noble et al., 2005; Phiel et al., 2003;

Pooler et al., 2012; White et al., 2006; Kimura et al., 2013). In double transgenic APP/tau mice, GSK-3 inhibition ameliorates plaque-related neuritic changes, suggesting a role of this kinase in Aβ-induced pathology (DaRocha-Souto et al., 2012). However, the molecular mechanisms linking Aβ oligomers toxicity to GSK-3 are still poorly understood. Our Western blot experiments demonstrating that $A\beta_{42}$ treatment markedly decreased the level of Ser-9 phosphorylated (inactive) GSK-3 (Fig. 5) are consistent with the emerging concept of a pathophysiological link between AD and altered GSK-3 signaling (Deng et al., 2014). Importantly, we discovered that treatment of hippocampal neurons with $A\beta_{42}$ results in GSK-3-dependent Kv4.2 phosphorylation at Ser-616 (Fig. 5). The Kv channel family includes the most heterogenous and abundant group of ion channels in excitable cells, comprising more than 40 subunit genes divided in separate families based on structural and functional properties (Gutman et al., 2003). So far, the only Kv channel subtype that has been validated as GSK-3 substrate is Kv7.2, which is encoded by the gene KCNQ2 (Jentsch, 2000). Here, we provide novel evidence for another Kv channel, Kv4.2, as a putative GSK-3 target.

A number of studies have demonstrated complex phosphorylation-dependent regulation of Kv4.2 with functional consequences on transient A-type K^+ currents. In vitro phosphorylation of recombinant fragments of Kv4.2 revealed PKA- (Anderson et al., 2000), ERK- (Adams et al., 2000), and CaMKII- (Varga et al., 2004) mediated phosphorylation of Kv4.2. It is noteworthy that ERK-mediated phosphorylation of Kv4.2 leads to decreased Kv4.2 and that ERK directly phosphorylates Kv4.2 at T602, T607, and Ser-616 (Schrader et al., 2006). The consensus sequence for GSK-3 targets typically consists of S/T-X-X-X-S/T in which the first S/T residue is the GSK-3 phosphorylation site flanked by a proline residue and followed by an S/T site (3 residues downstream), acting as a phosphorylation priming site (Jope and Johnson, 2004; Wildburger and Laezza, 2012). Ser-616 flanked by P617 and followed by S620 matches with a GSK-3 consensus motif (Fig. 7A). In support, we show that $A\beta_{42}$ treatment leads to increase Ser-616 phosphorylation of Kv4.2, an effect that is strongly attenuated by pharmacologic inhibition of GSK-3 (Fig. 7B) and is reproduced in 5-month-old 3xTg-AD brains (Fig. 8E). Altogether, these results support the notion that $A\beta_{42}$ induces a decrease of A-type K^+ currents and an increase in excitability through GSK-3-dependent phosphorylation of Kv4.2 at Ser-616.

The 5-month-old 3xTg-AD mouse model used in this study recapitulates early AD pathology, where endogenously produced Aβ accumulates inside neurons before the appearance of extracellular plaques (LaFerla et al., 2007; Oddo et al., 2003). Therefore, this model represents an elective tool for investigating the effects of intraneuronal Aβ accumulation. In support of a key role of iAβ in triggering early AD pathology, we found that hyperphosphorylation of Kv4.2 channels at Ser-616 was paralleled by increased firing and broadening of the AP of CA1 pyramidal neurons in 3xTg-AD mice (Fig. 8) similarly to what was observed in primary hippocampal neurons on iAβ exposure.

In animal models that overexpress Aβ, spontaneous network hyperexcitability has been documented (Born et al., 2014; Davis et al., 2014; Marcantoni et al., 2014; Minkeviciene et al., 2009; Palop et al., 2007). Data from the epilepsy literature inform us that similar hyperexcitability can arise from synaptic deficits, usually from unbalance between

excitatory and inhibitory transmission (Bateup et al., 2013) or changes in intrinsic excitability (McNamara et al., 2006). However, the deficits in synaptic function and plasticity described in Aβ overproducing mice (Randall et al., 2010) are unlikely the primary cause of hyperexcitability (Davis et al., 2014). Changes in neuronal membrane properties and intrinsic hyperexcitability in AD mouse models have been reported. Minkeviciene et al. (2009) identified an approximately 10 mV depolarizing shift in the membrane resting potential in layer II/III cortical pyramidal neurons of mice carrying human APPsve and PS1dE9 genes (APdE9 mice), whereas Brown et al., (2011) found enhanced excitability in CA1 pyramidal neurons of Aβ overproducing PSAPP double transgenic mice at 8 months of age. This effect was paralleled by an enhanced after-depolarizing potential and changes in the AP waveform, including reduced half-width. In a different model of Aβ overproducing mouse (CRDN8 mice), Wykes et al. (2012) found spikes in CA1 pyramidal neurons to be narrower, a finding in line with previous studies (Brown et al., 2011). On the contrary, in our experimental conditions, we found that the AP halfwidth was increased in 3xTg mice (Fig. 8). The reasons for this apparent discrepancy remains unclear, however, it is tempting to speculate that this may result from different age-dependent accumulation of intracellular versus extracellular $A\beta_{42}$ in various Aβ overproducing mouse models.

Our finding showing increased excitability of CA1 hippocampal pyramidal neurons in 3xTg-AD mice adds new insights into the mechanisms underlying $A\beta_{42}$-dependent network hyperexcitability further supporting a link between increased risk of seizures and AD. To this regard, it should be considered that although seizures are increased in the AD patients, overall epilepsy is not a common feature in AD (Amatniek et al., 2006; Palop and Mucke, 2009). Results from imaging scans, such as FDG-PET and/or SPECT brain scans, on AD patients, indicate reduced glucose utilization or blood flow in many brain regions, including hippocampus, supporting reduced resting brain activity (Ishii, 2013). According to these data, the expected increase in energy demand induced by neuronal hyperexcitability may be masked by the overall decrease in energy requirements caused by synaptic failures and neuronal loss.

Collectively, our results provide novel evidence for the role of intracellular Aβ accumulation in hyperexcitability observed in early AD and identify the Kv4.2 channel as a new endpoint of a caspase-dependent GSK-3 pathway and a potential therapeutic target for early AD treatment and prevention.

Supplementary Material

Refer to Web version on PubMed Central for supplementary material.

Acknowledgements

This work was supported by grants from Università Cattolica (D1-2012 #70200969 to Claudio Grassi and Marcello D'Ascenzo), Alzheimer's Association (NIRG-14-321307; to Cristian Ripoli), the Institute for Translational Sciences at the University of Texas Medical Branch as part of a Clinical and Translational Science Award (UL1TR000071, Fernanda Laezza) from the National Center for Advancing Translational Sciences, National Institutes of Health (NIH NIMH R01 MH095995 to Fernanda Laezza).

References

Adams JP, Anderson AE, Varga AW, Dineley KT, Cook RG, Pfaffinger PJ, Sweatt JD. The A-type potassium channel Kv4.2 is a substrate for the mitogen-activated protein kinase ERK. J. Neurochem. 2000; 75:2277–2287. [PubMed: 11080179]

Allen JW, Eldadah BA, Huang X, Knoblach SM, Faden AI. Multiple caspases are involved in β-amyloid-induced neuronal apoptosis. J. Neurosci. Res. 2001; 65:45–53. [PubMed: 11433428]

Amatniek JC, Hauser WA, DelCastillo-Castaneda C, Jacobs DM, Marder K, Albert M, Brandt J, Stern Y. Incidence and predictors of seizures in patients with Alzheimer's disease. Epilepsia. 2006; 47:867–872. [PubMed: 16686651]

Anderson AE, Adams JP, Qian Y, Cook RG, Pfaffinger PJ, Sweet JD. Kv4.2 phosphorylation by cyclic AMP-dependent protein kinase. J. Biol. Chem. 2000; 275:5337–5346. [PubMed: 10681507]

Attar A, Ripoli C, Riccardi E, Maiti P, Li Puma DD, Liu T, Hayes J, Jones MR, Lichti-Kaiser K, Yang F, Gale GD, Tseng CH, Tan M, Xie CW, Straudinger JL, Klärner FG, Schrader T, Frautschy SA, Grassi C, Bitan G. Protection of primary neurons and mouse brain from Alzheimer's pathology by molecular tweezers. Brain. 2012; 135:3735–3748. [PubMed: 23183235]

Bateup HS, Johnson CA, Denefrio CL, Saulnier JL, Kornacker K, Sabatini BL. Excitatory/inhibitory synaptic imbalance leads to hippocampal hyperexcitability in mouse models of tuberous sclerosis. Neuron. 2013; 78:510–522. [PubMed: 23664616]

Bonin RP, Martin LJ, MacDonald JF, Orser BA. Alpha5GABAA receptors regulatethe intrinsic excitability of mouse hippocampal pyramidal neurons. J. Neurophysiol. 2007; 98:2244–2254. [PubMed: 17715197]

Born HA, Kim JY, Savjani RR, Das P, Dabaghian YA, Guo Q, Yoo JW, Schuler DR, Cirrito JR, Zheng H, Golde TE, Noebels JL, Jankowsky JL. Genetic suppression of transgenic APP rescues hypersynchronous network activity in a mouse model of Alzheimer's disease. J. Neurosci. 2014; 34:3826–3840. [PubMed: 24623762]

Bradley CA, Peineau S, Taghibiglou C, Nicolas CS, Whitcomb DJ, Bortolotto ZA, Kaang BK, Cho K, Wang YT, Collingridge GL. A pivotal role of GSK-3 in synaptic plasticity. Front. Mol. Neurosci. 2012; 15:5–13.

Brown JT, Chin J, Leiser SC, Pangalos MN, Randall AD. Altered intrinsic neuronal excitability and reduced Na^+ currents in a mouse model of Alzheimer's disease. Neurobiol. Aging. 2011; 32:2109–2114. [PubMed: 21794952]

Busche MA, Chen X, Henning HA, Reichwald J, Staufenbiel M, Sakmann B, Konnerth A. Critical role of soluble amyloid-β for early hippocampal hyperactivity in a mouse model of Alzheimer's disease. Proc. Natl. Acad. Sci. U. S. A. 2012; 109:8740–8745. [PubMed: 22592800]

Chen C. β-Amyloid increases dendritic Ca^{2+} influx by inhibiting the A-type K^+ current in hippocampal CA1 pyramidal neurons. Biochem. Biophys. Res. Commun. 2005; 338:1913–1919. [PubMed: 16289381]

Cho JH, Johnson GV. Glycogen synthase kinase 3 b induces caspase-cleaved tau aggregation in situ. J. Biol. Chem. 2004; 279:54716–54723. [PubMed: 15494420]

Chong YH, Shin YJ, Lee EO, Kayed R, Glabe CG, Tenner AJ. ERK1/2 activation mediates Aβ oligomer-induced neurotoxicity via caspase-3 activation and tau cleavage in rat organotypic hippocampal slice cultures. J. Biol. Chem. 2006; 281:20315–20325. [PubMed: 16714296]

Carrasquillo Y, Burkhalter A, Nerbonne JM. A-type K^+ channels encoded by Kv4.2, Kv4.3 and Kv1.4 differentially regulate intrinsic excitability of cortical pyramidal neurons. J. Physiol. 2012; 590:3877–3890. [PubMed: 22615428]

Citron M. Alzheimer's disease: strategies for disease modification. Nat. Rev. Drug Discov. 2010; 9:387–398. [PubMed: 20431570]

Clementi ME, Pezzotti M, Orsini F, Sampaolese B, Mezzogori D, Grassi C, Giardina B, Giardina B, Misiti F. Alzheimer's amyloid β-peptide (1-42) induces cell death in human neuroblastoma via bax/bcl-2 ratio increase: an intriguing role for methionine 35. Biochem. Biophys. Res. Commun. 2006; 342:206–213. [PubMed: 16472763]

Coetzee WA, Amarillo Y, Chiu J, Chow A, Lau D, McCormack T. Molecular diversity of K^+ channels. Ann. N. Y. Acad. Sci. 1999; 868:233–285. [PubMed: 10414301]

Crimins JL, Pooler A, Polydoro M, Luebke JI, Spires-Jones TL. The intersection of amyloid b and tau in glutamatergic synaptic dysfunction and collapse in Alzheimer's disease. Ageing Res. Rev. 2013; 12:757–763. [PubMed: 23528367]

Curcio L, Podda MV, Leone L, Piacentini R, Mastrodonato A, Cappelletti P, Sacchi S, Pollegioni L, Grassi C, D'Ascenzo M. Reduced D-serine levels in the nucleus accumbens of cocaine-treated rats hinder the induction of NMDA receptor-dependent synaptic plasticity. Brain. 2013; 136:1216–1230. [PubMed: 23518710]

D'Amelio M, Rossini PM. Brain excitability and connectivity of neuronal assemblies in Alzheimer's disease: from animal models to human findings. Prog. Neurobiol. 2012; 99:42–60. [PubMed: 22789698]

DaRocha-Souto B, Coma M, Pérez-Nievas BG, Scotton TC, Siao M, Sánchez-Ferrer P, Hashimoto T, Fan Z, Hudry E, Barroeta I, Serenó L, Rodríguez M, Sánchez MB, Hyman BT, Gómez-Isla T. Activation of glycogen synthase kinase-3 β mediates β-amyloid induced neuritic damage in Alzheimer's disease. Neurobiol. Dis. 2012; 45:425–437. [PubMed: 21945540]

D'Ascenzo M, Podda MV, Fellin T, Azzena GB, Haydon P, Grassi C. Activation of mGluR5 induces spike after depolarization and enhanced excitability in medium spiny neurons of the nucleus accumbens by modulating persistent Na^+ currents. J. Physiol. 2009; 587:3233–3250. [PubMed: 19433572]

Davis KE, Fox S, Gigg J. Increased hippocampal excitability in the 3xTgAD mouse model for Alzheimer's disease in vivo. PLoS One. 2014; 9:e91203. [PubMed: 24621690]

Del Vecchio RA, Gold LH, Novick SJ, Wong G, Hyde LA. Increased seizure threshold and severity in young transgenic CRND8 mice. Neurosci. Lett. 2004; 367:164–167. [PubMed: 15331144]

Deng Y, Xiong Z, Chen P, Wei J, Chen S, Yan Z. β-Amyloid impairs the regulation of N-methyl-D-aspartate receptors by glycogen synthase kinase 3. Neurobiol. Aging. 2014; 35:449–459. [PubMed: 24094580]

Emamian ES, Hall D, Birnbaum MJ, Karayiorgou M, Gogos JA. Convergent evidence for impaired AKT1-GSK-3b signaling in schizophrenia. Nat. Genet. 2004; 36:131–137. [PubMed: 14745448]

Frame S, Cohen P. GSK3 takes centre stage more than 20 years after its discovery. Biochem. J. 2001; 359:1–16. [PubMed: 11563964]

Good TA, Murphy RM. Effect of β-amyloid block of the fast-inactivating K^+ channel on intracellular Ca^{2+} and excitability in a modeled neuron. Proc. Natl. Acad. Sci. U. S. A. 1996; 93:15130–15135. [PubMed: 8986775]

Gouras GK, Tsai J, Naslund J, Vincent B, Edgar M, Checler F, Greenfield JP, Haroutunian V, Buxbaum JD, Xu H, Greengard P, Relkin NR. Intraneuronal Ab_{42} accumulation in human brain. Am. J. Pathol. 2000; 156:15–20. [PubMed: 10623648]

Gouras GK, Willén K, Tampellini D. Critical role of intraneuronal Aβ in Alzheimer's disease: technical challenges in studying intracellular Aβ. Life Sci. 2012; 91:1153–1158. [PubMed: 22727791]

Grassi C, D'Ascenzo M, Azzena GB. Modulation of Ca(v)1 and Ca(v)2.2 channels induced by nitric oxide via cGMP-dependent protein kinase. Neurochem. Int. 2004; 45:885–893. [PubMed: 15312983]

Gutman GA, Chandy KG, Adelman JP, Aiyar J, Bayliss DA, Clapham DE, Covarriubias M, Desir GV, Furuichi K, Ganetzky B, Garcia ML, Grissmer S, Jan LY, Karschin A, Kim D, Kuperschmidt S, Kurachi Y, Lazdunski M, Lesage F, Lester HA, McKinnon D, Nichols CG, O'Kelly I, Robbins J, Robertson GA, Rudy B, Sanguinetti M, Seino S, Stuehmer W, Tamkun MM, Vandenberg CA, Wei A, Wulff H, Wymore RS. International Union of Pharmacology. XLI. Compendium of voltage-gated ion channels: potassium channels. Pharmacol. Rev. 2003; 55:583–586. [PubMed: 14657415]

Guzmán EA, Bouter Y, Richard BC, Lannfelt L, Ingelsson M, Paetau A, Verkkoniemi-Ahola A, Wirths O, Bayer TA. Abundance of Ab5-x like immunoreactivity in transgenic 5XFAD, APP/PS1KI and 3xTG mice, sporadic and familial Alzheimer's disease. Mol. Neurodegener. 2014; 9:13. [PubMed: 24694184]

Gylys KH, Fein JA, Tan AM, Cole GM. Apolipoprotein E enhances uptake of soluble but not aggregated amyloid-β protein into synaptic terminals. J. Neurochem. 2003; 84:1442–1451. [PubMed: 12614344]

Hardy J, Selkoe DJ. The amyloid hypothesis of Alzheimer's disease: progress and problems on the road to therapeutics. Science. 2002; 297:353–356. [PubMed: 12130773]

Heneka MT, Kummer MP, Stutz A, Delekate A, Schwartz S, Vieira-Saecker A, Griep A, Axt D, Remus A, Tzeng TC, Gelpi E, Halle A, Korte M, Latz E, Golenbock DT. NLRP3 is activated in Alzheimer's disease and contributes to pathology in APP/PS1 mice. Nature. 2013; 493:674–678. [PubMed: 23254930]

Hoffman DA, Johnston D. Downregulation of transient K^+ channels in dendrites of hippocampal CA1 pyramidal neurons by activation of PKA and PKC. J. Neurosci. 1998; 18:3521–3528. [PubMed: 9570783]

Hommet C, Mondon K, Camus V, De Toffol B, Constans T. Epilepsy and dementia in the elderly. Dement. Geriatr. Cogn. Disord. 2008; 25:293–300. [PubMed: 18311076]

Hu HJ, Carrasquillo Y, Karim F, Jung WE, Nerbonne JM, Schwarz TL, Gereau RW. The Kv4.2 potassium channel subunit is required for pain plasticity. Neuron. 2006; 50:89–100. [PubMed: 16600858]

Ishii K. PET approaches for diagnosis of dementia. AJNR Am. J. Neuroradiol. 2013; 9:13.

Jarrett JT, Berger EP, Lansbury PT Jr. The carboxy terminus of the β amyloid protein is critical for the seeding of amyloid formation: implications for the pathogenesis of Alzheimer's disease. Biochemistry. 1993; 32:4693–4697. [PubMed: 8490014]

Jentsch TJ. Neuronal KCNQ potassium channels: physiology and role in disease. Nat. Rev. Neurosci. 2000; 1:21–30. [PubMed: 11252765]

Jo J, Whitcomb DJ, Olsen KM, Kerrigan TL, Lo SC, Bru-Mercier G, Dickinson B, Scullion S, Sheng M, Collingridge G, Cho K. Aβ(1-42) inhibition of LTP is mediated by a signaling pathway involving caspase-3, Akt1 and GSK-3β. Nat. Neurosci. 2011; 14:545–547. [PubMed: 21441921]

Jope RS, Johnson GV. The glamour and gloom of glycogen synthase kinase-3. Trends. Biochem. Sci. 2004; 29:95–102. [PubMed: 15102436]

Kapfhamer D, Berger KH, Hopf FW, Seif T, Kharazia V, Bonci A, Heberlein U. Protein phosphatase 2a and glycogen synthase kinase 3 signaling modulate prepulse inhibition of the acoustic startle response by altering cortical M-type potassium channel activity. J. Neurosci. 2010; 30:8830–8840. [PubMed: 20592205]

Kim E, Hoffman DA. Dynamic regulation of synaptic maturation state by voltage-gated A type K^+ channels in CA1 hippocampal pyramidal neurons. J. Neurosci. 2012; 32:14427–14432. [PubMed: 23055512]

Kim J, Basak JM, Holtzman DM. The role of apolipoprotein E in Alzheimer's disease. Neuron. 2009; 63:287–303. [PubMed: 19679070]

Kim J, Wei DS, Hoffman DA. Kv4 potassium channel subunits control action potential repolarization and frequency-dependent broadening in rat hippocampal CA1 pyramidal neurones. J. Physiol. 2005; 569:41–57. [PubMed: 16141270]

Kimura T, Whitcomb DJ, Jo J, Regan P, Piers T, Heo S, Brown C, Hashikawa T, Murayama M, Seok H, Sotiropoulos I, Kim E, Collingridge GL, Takashima A, Cho K. Microtubule-associated protein tau is essential for long-term depression in the hippocampus. Philos. Trans. R. Soc. Lond. B Biol. Sci. 2013; 369 20130144.

Klyubin I, Cullen WK, Hu NW, Rowan MJ. Alzheimer's disease Aβ assemblies mediating rapid disruption of synaptic plasticity and memory. Mol. Brain. 2012; 17:5–25.

Klyubin I, Walsh DM, Lemere CA, Cullen WK, Shankar GM, Betts V, Spooner ET, Jiang L, Anwyl R, Selkoe DJ, Rowan MJ. Amyloid β protein immunotherapy neutralizes Aβ oligomers that disrupt synaptic plasticity in vivo. Nat. Med. 2005; 11:556–561. [PubMed: 15834427]

Kuo YM, Beach TG, Sue LI, Scott S, Layne KJ, Kokjohn TA, Kalback WM, Luehrs DC, Vishnivetskaya TA, Abramowski D, Sturchler-Pierrat C, Staufenbiel M, Weller RO, Roher AE. The evolution of Aβ peptide burden in the APP23 transgenic mice: implications for Aβ deposition in Alzheimer disease. Mol. Med. 2001; 7:609–618. [PubMed: 11778650]

Kuszczyk MA, Sanchez S, Pankiewicz J, Kim J, Duszczyk M, Guridi M, Guridi M, Asuni AA, Sullivan PM, Holtzman DM, Sadowski MJ. Blocking the interaction between apolipoprotein E and Aβ reduces intraneuronal accumulation of Aβ and inhibits synaptic degeneration. Am. J. Pathol. 2013; 182:1750–1768. [PubMed: 23499462]

LaFerla FM, Green KN, Oddo S. Intracellular amyloid-β in Alzheimer's disease. Nat. Rev. Neurosci. 2007; 8:499–509. [PubMed: 17551515]

Li Z, Sheng M. Caspases in synaptic plasticity. Mol. Brain. 2012; 14:5–15.

Lin L, Sun W, Kung F, Dell'Acqua ML, Hoffman DA. AKAP79/150 impacts intrinsic excitability of hippocampal neurons through phospho-regulation of A-type K^+ channel trafficking. J. Neurosci. 2011; 31:1323–1332. [PubMed: 21273417]

Liu Q, Xie X, Lukas RJ, St John PA, Wu J. A novel nicotinic mechanism underlies β-amyloid-induced neuronal hyperexcitation. J. Neurosci. 2013; 33:7253–7263. [PubMed: 23616534]

Louneva N, Cohen JW, Han LY, Talbot K, Wilson RS, Bennett DA, Trojanowski JQ, Arnold SE. Caspase-3 is enriched in postsynaptic densities and increased in Alzheimer's. Am. J. Pathol. 2008; 73:1488–1495. [PubMed: 18818379]

Lucas FR, Goold RG, Gordon-Weeks PR, Salinas PC. Inhibition of GSK-3b leading to the loss of phosphorylated MAP-1B is an early event in axonal remodelling induced by WNT-7a or lithium. J. Cell. Sci. 1998; 111:1351–1361. [PubMed: 9570753]

Marcantoni A, Raymond EF, Carbone E, Marie H. Firing properties of entorhinal cortex neurons and early alterations in an Alzheimer's disease transgenic model. Pflugers Arch. 2014; 466:1437–1450. [PubMed: 24132829]

Mattson MP. Pathways towards and away from Alzheimer's disease. Nature. 2004; 430:631–639. [PubMed: 15295589]

McDermott CM, Schrader LA. Activation of κ opioid receptors increases intrinsic excitability of dentate gyrus granule cells. J. Physiol. 2011; 589:3517–3532. [PubMed: 21606111]

McNamara JO, Huang YZ, Leonard AS. Molecular signaling mechanisms underlying epileptogenesis. Sci. STKE. 2006; 356:re12. [PubMed: 17033045]

Medina M, Avila J. Understanding the relationship between GSK-3 and Alzheimer's disease: a focus on how GSK-3 can modulate synaptic plasticity processes. Expert Rev. Neurother. 2013; 13:495–503. [PubMed: 23621307]

Minkeviciene R, Rheims S, Dobszay MB, Zilberter M, Hartikainen J, Fülöp L, Penke B, Zilberter Y, Harkany T, Pitkänen A, Tanila H. Amyloid β-induced neuronal hyperexcitability triggers progressive epilepsy. J. Neurosci. 2009; 29:3453–3462. [PubMed: 19295151]

Mitterdorfer J, Bean BP. Potassium currents during the action potential of hippocampal CA3 neurons. J. Neurosci. 2002; 22:10106–10115. [PubMed: 12451111]

Mori C, Spooner ET, Wisniewsk KE, Wisniewski TM, Yamaguch H, Saido TC, Tolan DR, Selkoe DJ, Lemere CA. Intraneuronal Aβ42 accumulation in Down syndrome brain. Amyloid. 2002; 9:88–102. [PubMed: 12440481]

Mucke L, Selkoe DJ. Neurotoxicity of amyloid β-protein: synaptic and network dysfunction. Cold Spring Harb. Perspect.Med. 2012; 2:a006338. [PubMed: 22762015]

Nicholson DW. Caspase structure, proteolytic substrates, and function during apoptotic cell death. Cell. Death Differ. 1999; 6:1028–1042. [PubMed: 10578171]

Noble W, Planel E, Zehr C, Olm V, Meyerson J, Suleman F, Gaynor K, Wang L, LaFrancois J, Feinstein B, Burns M, Krishnamurthy P, Wen Y, Bhat R, Lewis J, Dickson D, Duff K. Inhibition of glycogen synthase kinase-3 by lithium correlates with reduced tauopathy and degeneration in vivo. Proc. Natl. Acad. Sci. U. S. A. 2005; 102:6990–6995. [PubMed: 15867159]

Oakley H, Cole SL, Logan S, Maus E, Shao P, Craft J, Guillozet-Bongaarts A, Ohno M, Disterhoft J, Van Eldik L, Berry R, Vassar R. Intraneuronal β-amyloid aggregates, neurodegeneration, and neuron loss in transgenic mice with five familial Alzheimer's disease mutations: potential factors in amyloid plaque formation. J. Neurosci. 2006; 26:10129–10140. [PubMed: 17021169]

Oddo S, Caccamo A, Shepherd JD, Murphy MP, Golde TE, Kayed R, Metherate R, Mattson MP, Akbari Y, LaFerla FM. Triple-transgenic model of Alzheimer's disease with plaques and tangles: intracellular Aβ and synaptic dysfunction. Neuron. 2003; 39:409–421. [PubMed: 12895417]

Palop JJ, Chin J, Roberson ED, Wang J, Thwin MT, Bien-Ly N, Yoo J, Ho KO, Yu GQ, Kreitzer A, Finkbeiner S, Noebels JL, Mucke L. Aberrant excitatory neuronal activity and compensatory remodeling of inhibitory hippocampal circuits in mouse models of Alzheimer's disease. Neuron. 2007; 55:697–711. [PubMed: 17785178]

Palop JJ, Mucke L. Epilepsy and cognitive impairments in Alzheimer disease. Arch. Neurol. 2009; 66:435–440. [PubMed: 19204149]

Phiel CJ, Wilson CA, Lee VM, Klein PS. GSK-3alpha regulates production of Alzheimer's disease amyloid-β peptides. Nature. 2003; 423:435–439. [PubMed: 12761548]

Penke B, Tóth AM, Földi I, Szücs M, Janáky T. Intraneuronal β-amyloid and its interactions with proteins and subcellular organelles. Electrophoresis. 2012; 33:3608–3616. [PubMed: 23161402]

Piacentini R, Ripoli C, Leone L, Misiti F, Clementi ME, D'Ascenzo M, Giardina B, Azzena GB, Grassi C. Role of methionine 35 in the intracellular Ca^{2+} homeostasis dysregulation and Ca^{2+}-dependent apoptosis induced by amyloid β-peptide in human neuroblastoma IMR32 cells. J. Neurochem. 2008; 107:1070–1082. [PubMed: 18990116]

Podda MV, D'Ascenzo M, Leone L, Piacentini R, Azzena GB, Grassi C. Functional role of cyclic nucleotide-gated channels in rat medial vestibular nucleus neurons. J. Physiol. 2008; 5863:803–815. [PubMed: 18048449]

Podda MV, Leone L, Piacentini R, Cocco S, Mezzogori D, D'Ascenzo, Grassi C. Expression of olfactory-type cyclic nucleotide-gated channels in rat cortical astrocytes. Glia. 2012; 60:1391–1405. [PubMed: 22653779]

Podda MV, Marcocci ME, Oggiano L, D'Ascenzo M, Tolu E, Palamara AT, Azzena GB, Grassi C. Nitric oxide increases the spontaneous firing rate of rat medial vestibular nucleus neurons in vitro via a cyclic GMP-mediated PKG-independent mechanism. Eur. J. Neurosci. 2004; 20:2124–2132. [PubMed: 15450091]

Pooler AM, Usardi A, Evans CJ, Philpott KL, Noble W, Hanger DP. Dynamic association of tau with neuronal membranes is regulated by phosphorylation. Neurobiol. Aging. 2012; 431:27–38.

Putcha D, Brickhouse M, O'Keefe K, Sullivan C, Rentz D, Marshall G, Dickerson B, Sperling R. Hippocampal hyperactivation associated with cortical thinning in Alzheimer's disease signature regions in non-demented elderly adults. J. Neurosci. 2011; 31:17680–17688. [PubMed: 22131428]

Randall AD, Witton J, Booth C, Hynes-Allen A, Brown JT. The functional neurophysiology of the amyloid precursor protein (APP) processing pathway. Neuropharmacology. 2010; 59:243–267. [PubMed: 20167227]

Ripoli C, Piacentini R, Riccardi E, Leone L, Li Puma DD, Bitan G, Grassi C. Effects of different amyloid β-protein analogues on synaptic function. Neurobiol. Aging. 2013; 34:1032–1044. [PubMed: 23046860]

Ripoli C, Cocco S, Li Puma DD, Piacentini R, Mastrodonato A, Scala F, D'ascenzo M, Grassi C. Intracellular accumulation of amyloid-β (Aβ) protein plays a major role in Aβ-induced alterations of glutamatergic synaptic transmission and plasticity. J. Neurosci. 2014; 34:12893–12903. [PubMed: 25232124]

Rohn TT. The role of caspases in Alzheimer's disease; potential novel therapeutic opportunities. Apoptosis. 2010; 15:1403–1409. [PubMed: 20127416]

Schrader LA, Birnbaum SG, Nadin BM, Ren Y, Bui D, Anderson AE, Sweatt JD. ERK/MAPK regulates the Kv4.2 potassium channel by direct phosphorylation of the pore-forming subunit. Cell. Physiol. 2006; 290:852–861.

Selkoe DJ. Alzheimer's disease is a synaptic failure. Science. 2002; 298:789–791. [PubMed: 12399581]

Selkoe DJ. Alzheimer's disease results from the cerebral accumulation and cytotoxicity of amyloid β-protein. J. Alzheimers. Dis. 2001; 3:75–80. [PubMed: 12214075]

Shankar GM, Li S, Mehta TH, Garcia-Munoz A, Shepardson NE, Smith I, Brett FM, Farrell MA, Rowan MJ, Lemere CA, Regan CM, Walsh DM, Sabatini BL, Selkoe DJ. Amyloid-β protein dimers isolated directly from Alzheimer's brains impair synaptic plasticity and memory. Nat. Med. 2008; 14:837–842. [PubMed: 18568035]

Sheng M, Sabatini BL, Südhof TC. Synapses and Alzheimer's disease. Cold Spring Harb. Perspect. Biol. 2012; 4:a005777. [PubMed: 22491782]

Snigdha S, Smith ED, Prieto GA, Cotman CW. Caspase-3 activation as a bifurcation point between plasticity and cell death. Neurosci. Bull. 2012; 28:14–24. [PubMed: 22233886]

Steinerman JR, Irizarry M, Scarmeas N, Raju S, Brandt J, Albert M, Blacker D, Hyman B, Stern Y. Distinct pools of β-amyloid in Alzheimer disease-affected brain: a clinicopathologic study. Arch. Neurol. 2008; 65:906–912. [PubMed: 18625856]

Sultana R, Banks WA, Butterfield DA. Decreased levels of PSD95 and two associated proteins and increased levels of BCl_2 and caspase 3 in hippocampus from subjects with amnestic mild cognitive impairment: insights into their potential roles for loss of synapses and memory, accumulation of Aβ, and neurodegeneration in a prodromal stage of Alzheimer's disease. J. Neurosci. Res. 2010; 88:469–477. [PubMed: 19774677]

Takahashi RH, Capetillo-Zarate E, Lin MT, Milner TA, Gouras GK. Co-occurrence of Alzheimer's disease β-amyloid and tau pathologies at synapses. Neurobiol. Aging. 2014; 31:1145–1152. [PubMed: 18771816]

Takashima A, Noguchi K, Sato K, Hoshino T, Imahori K. Tau protein kinase I is essential for amyloid β-protein-induced neurotoxicity. Proc. Natl. Acad. Sci. U. S. A. 1993; 90:7789–7793. [PubMed: 8356085]

Takashima A. GSK-3 is essential in the pathogenesis of Alzheimer's disease. J. Alzheimers Dis. 2006; 9:309–317. [PubMed: 16914869]

Tampellini D, Magrané J, Takahashi RH, Li F, Lin MT, Almeida CG, Gouras GK. Internalized antibodies to the Aβ domain of APP reduce neuronal Aβ and protect against synaptic alterations. J. Biol. Chem. 2007; 282:18895–18906. [PubMed: 17468102]

Thinakaran G, Koo EH. Amyloid precursor protein trafficking, processing, and function. J. Biol. Chem. 2008; 283:29615–29619. [PubMed: 18650430]

Varga AW, Anderson AE, Adams JP, Vogel H, Sweatt JD. Input-specific immunolocalization of differentially phosphorylated Kv4.2 in the mouse brain. Learn. Mem. 2000; 7:321–332. [PubMed: 11040264]

Varga AW, Yuan LL, Anderson AE, Schrader LA, Wu GY, Gatchel JR, Johnston D, Sweatt JD. Calcium-calmodulin-dependent kinase II modulates Kv4.2 channel expression and upregulates neuronal A-type potassium currents. J. Neurosci. 2004; 24:3643–3654. [PubMed: 15071113]

White AR, Du T, Laughton KM, Volitakis I, Sharples RA, Xilinas ME, Hoke DE, Holsinger RM, Evin G, Cherny RA, Hill AF, Barnham KJ, Li QX, Bush AI, Masters CL. Degradation of the Alzheimer disease amyloid β-peptide by metal-dependent up-regulation of metalloprotease activity. J. Biol. Chem. 2006; 281:17670–17680. [PubMed: 16648635]

Wildburger NC, Laezza F. Control of neuronal ion channel function by glycogen synthase kinase-3: new prospective for an old kinase. Front. Mol. Neurosci. 2012; 5:80. [PubMed: 22811658]

Wykes R, Kalmbach A, Elia va M, Waters J. Changes in physiology of CA1 hippocampal pyraidasl neurons in preplaque CRMD8 mice. Neurbiol. Agng. 2012; 33:1609–1623.

Yamamoto K, Ueta Y, Wang L, Yamamoto R, Inoue N, Inokuchi K, Aiba A, Yonekura H, Kato N. Suppression of a neocortical potassium channel activity by intracellular amyloid-β and its rescue with Homer1a. J. Neurosci. 2011; 31:11100–11109. [PubMed: 21813671]

Ye CP, Selkoe DJ, Hartley DM. Protofibrils of amyloid β-protein inhibit specific K^+ currents in neocortical cultures. Neurobiol. Dis. 2003; 13:177–190. [PubMed: 12901832]

Youmans KL, Tai LM, Kanekiyo T, Stine WB Jr. Michon SC, Manelli AM, Fu Y, Riordan S, Eimer WA, Binder L, Bu G, Yu C, Hartley DM, LaDu MJ. Intraneuronal Aβ detection in 5xFAD mice by a new Aβ-specific antibody. Mol. Neurodegener. 2012; 7:8. [PubMed: 22423893]

Zepa L, Frenkel M, Belinson H, Kariv-Inbal Z, Kayed R, Masliah E, Michaelson DM. ApoE4-driven accumulation of intraneuronal oligomerized Aβ42 following activation of the amyloid cascade in vivo is mediated by a gain of function. Int J. Alzheimers. Dis. 2011; 5:792070. [PubMed: 21350674]

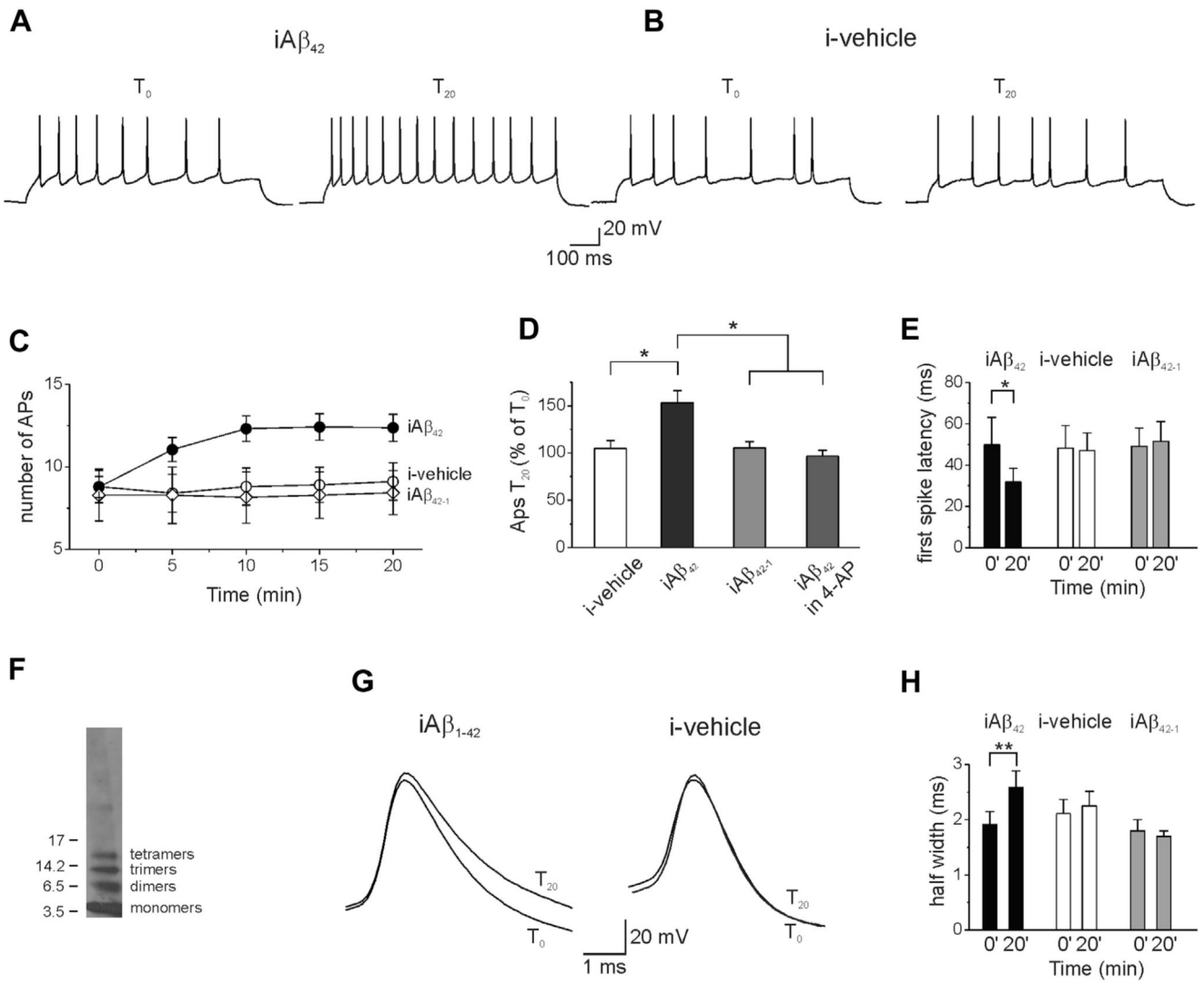

Fig. 1.

Intracellular perfusion of $A\beta_{42}$ increases primary hippocampal neuron excitability. (A) Whole-cell recordings from a hippocampal neuron in current-clamp configuration showing the increase in APs number after 20 minutes of intracellular perfusion of $A\beta_{42}$ via the patch pipette. (B) Intracellular vehicle perfusion had no effect on neuronal excitability. (C) Time course of the APs number recorded during intracellular perfusion of $A\beta_{42}$ (n = 22), vehicle (n = 10), and the reverse protein $A\beta_{42\text{-}1}$ (n = 7). (D) Bar graph summarizing data from experiments shown in C. Multiple comparisons were performed with ANOVA test with Tukey post hoc ($F_{(3,40)} = 5.47$; $^*p < 0.05$). Data are expressed as percentage of APs number recorded after 20 minutes of intracellular perfusion of either vehicle or $A\beta_s$ (T_{20}) versus that recorded soon after establishing the whole-cell configuration (T_0). (E) Bar graph showing first spike latency in different experimental conditions (n = 22). (F) Representative Western blot of recombinant $A\beta_{42}$ (200 nM) incubated for 18 hours at 4 °C used in this study. (G) Representative traces showing the AP width in either an $A\beta_{42}$-injected (left) or a vehicle-injected neuron (right). Recordings, at T_0 and T_{20}, are superimposed to clarify the spike

broadening in $A\beta_{42}$-injected neurons. (H) Bar graph showing mean values of spike half-width after 20 minutes of intracellular perfusion of $A\beta_{42}$ (n = 10), vehicle (n = 10), and $iA\beta_{42\text{-}1}$ (n = 7). Error bars indicate SEM, *$p < 0.05$; ** $p < 0.001$ in this and in the following figures. Abbreviations: Aβ, amyloid β-protein; ANOVA, analysis of variance; APs, action potentials; iAβ, intracellular Aβ; SEM, standard errors of the means.

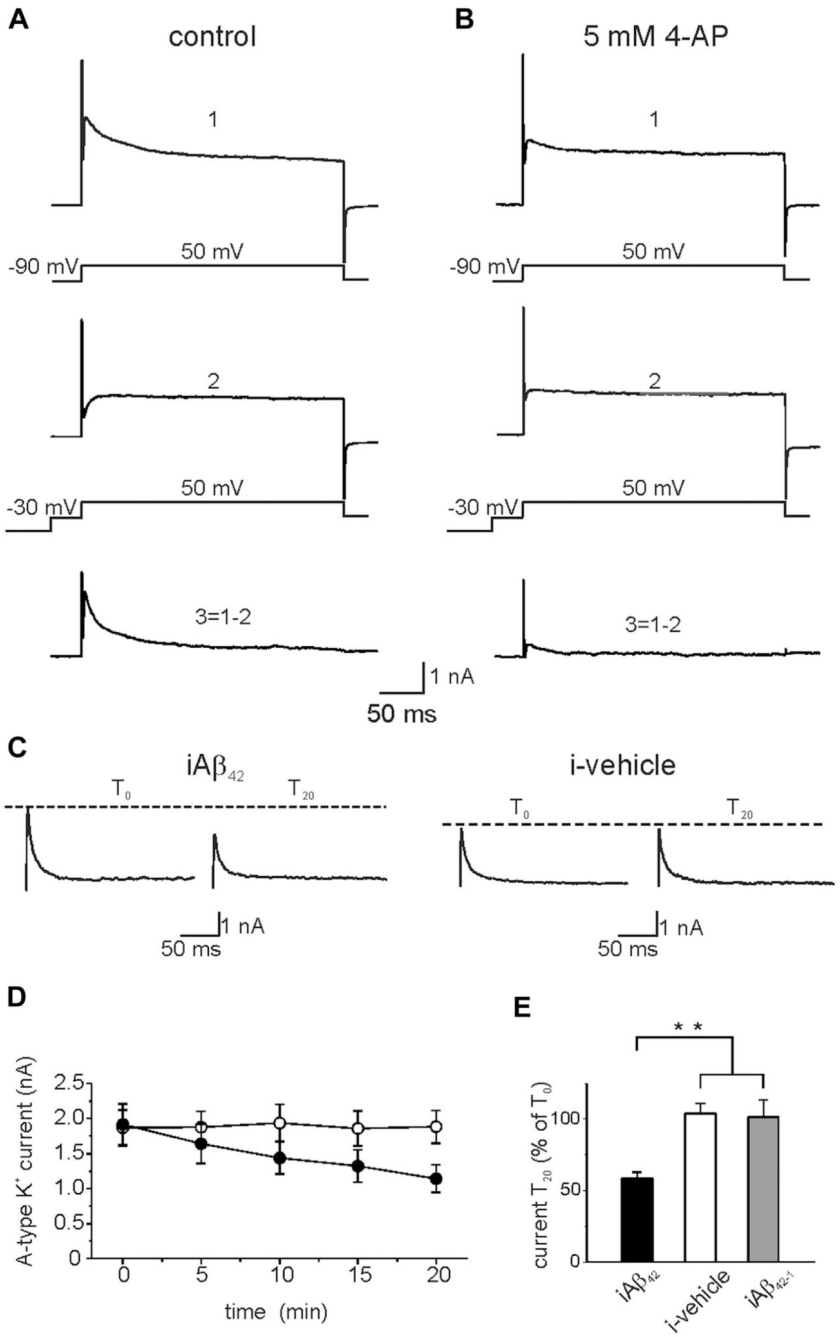

Fig. 2.

Intracellular $A\beta_{42}$ reduces transient A-type K+ currents in primary hippocampal neurons. (A) Isolation of the transient A-type K^+ current from a hippocampal neuron in the voltage-clamp configuration. The total outward current (upper trace; 1) was recorded during 300 ms voltage steps from −90 to +50 mV. To inactivate the transient K^+ channel a prepulse to −30 mV (50 ms) was applied before the voltage step to +50 mV (middle trace; 2). The transient K^+ current (lower trace; 3) was isolated by digital subtraction of the sustained current from the total outward current. (B) K^+ current recorded in the presence of 5 mM of 4-APs, an A-

type K^+ current blocker (from the same neuron shown in A). (C) Representative traces showing the effect of 20 minutes intracellular application of $A\beta_{42}$ (left) or vehicle (right). (D) Time course of the transient A-type K^+ current amplitudes during intracellular perfusion of $A\beta_{42}$ (black circles; n = 10) and vehicle (open circles; n = 10). (E) Bar graph summarizing data from experiments shown in C (average transient A-type K^+ current at T_{20} is expressed as percentage of transient A-type K^+ current recorded at T0; iAβ42 *n* = 11; i-vehicle *n* = 10; iAβ42-1 *n* = 6; ** $p < 0.001$). Abbreviations: Aβ, amyloid β-protein; APs, action potentials.

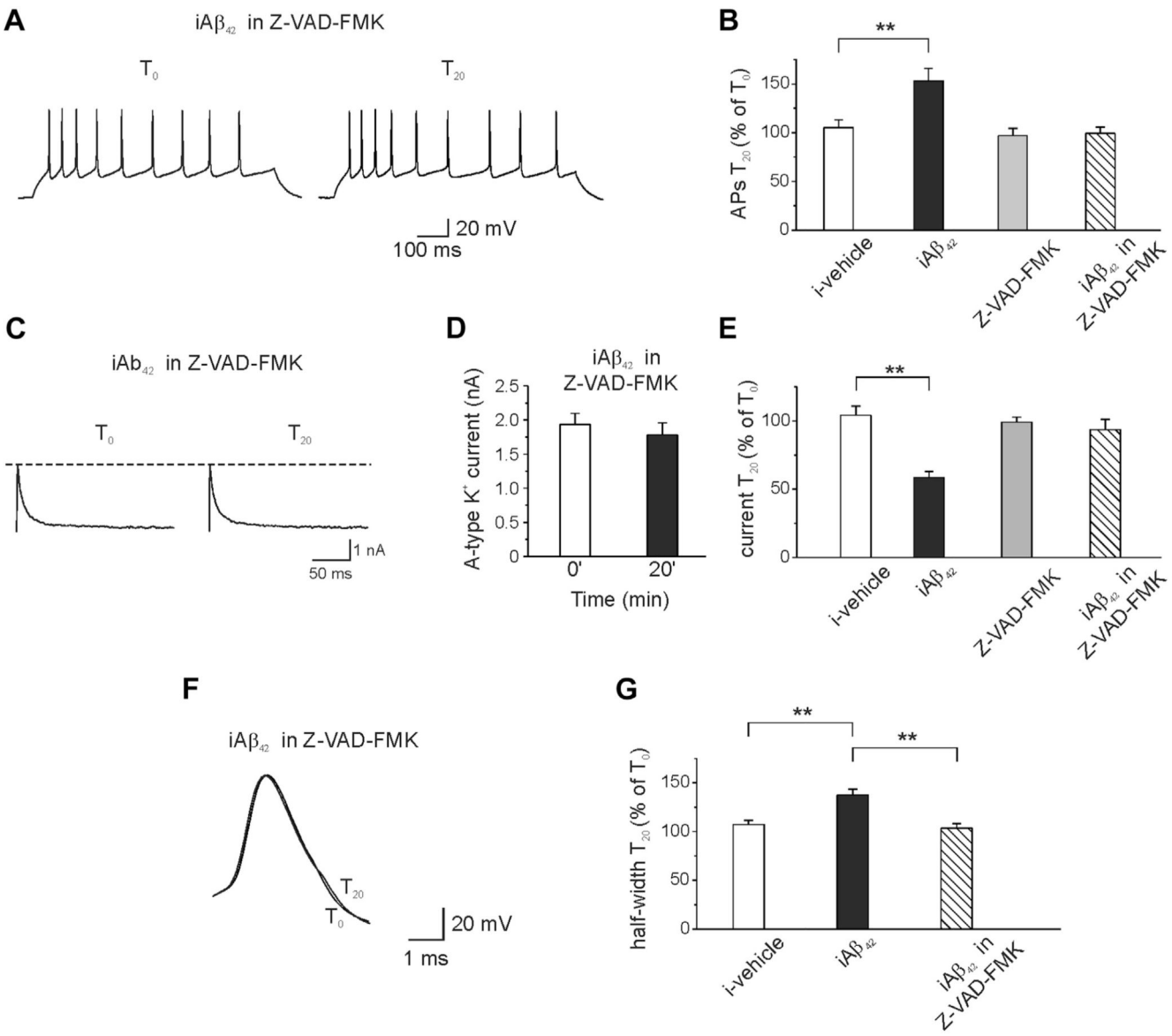

Fig. 3.

Preincubation of the neurons with the pan-caspase inhibitor Z-VAD-FMK prevents iAβ_{42}-induced increase in membrane excitability. (A) Representative traces showing no effect of iAβ_{42} on membrane excitability when neurons were preincubated (20 minutes) with the pan-caspase inhibitor Z-VAD-FMK (50 μM). (B) Bar graph summarizing data from experiments shown in A (ANOVA test with Tukey post hoc; $F_{(3,42)} = 5.50$; $^{**}p < 0.001$). Note that Z-VAD-FMK itself had no effect on membrane excitability (n = 10). For comparison the effect of vehicle and iAβ_{42} are shown (same data of Fig. 1). (C) Representative traces showing that iAβ_{42} had no effect on the transient A-type K^+ current when neurons were preincubated with Z-VAD-FMK. (D) Bar graph showing the mean current amplitudes in the 2 different conditions. (E) Bar graph summarizing data for the transient A-type K^+ current experiments (ANOVA test with Tukey post hoc; $F_{(3,33)} = 12.8$; $^{**}p < 0.001$). (F) Preincubation of neurons with Z-VAD-FMK also prevented the iAβ_{42}-induced increase in spike broadening

(n = 8). (G) Bar graph summarizing data from experiments shown in F (ANOVA test with Tukey post hoc; $F_{(2,24)} = 14.5$; $^{**}p < 0.001$). Abbreviations: ANOVA, analysis of variance; iAβ, intracellular Aβ.

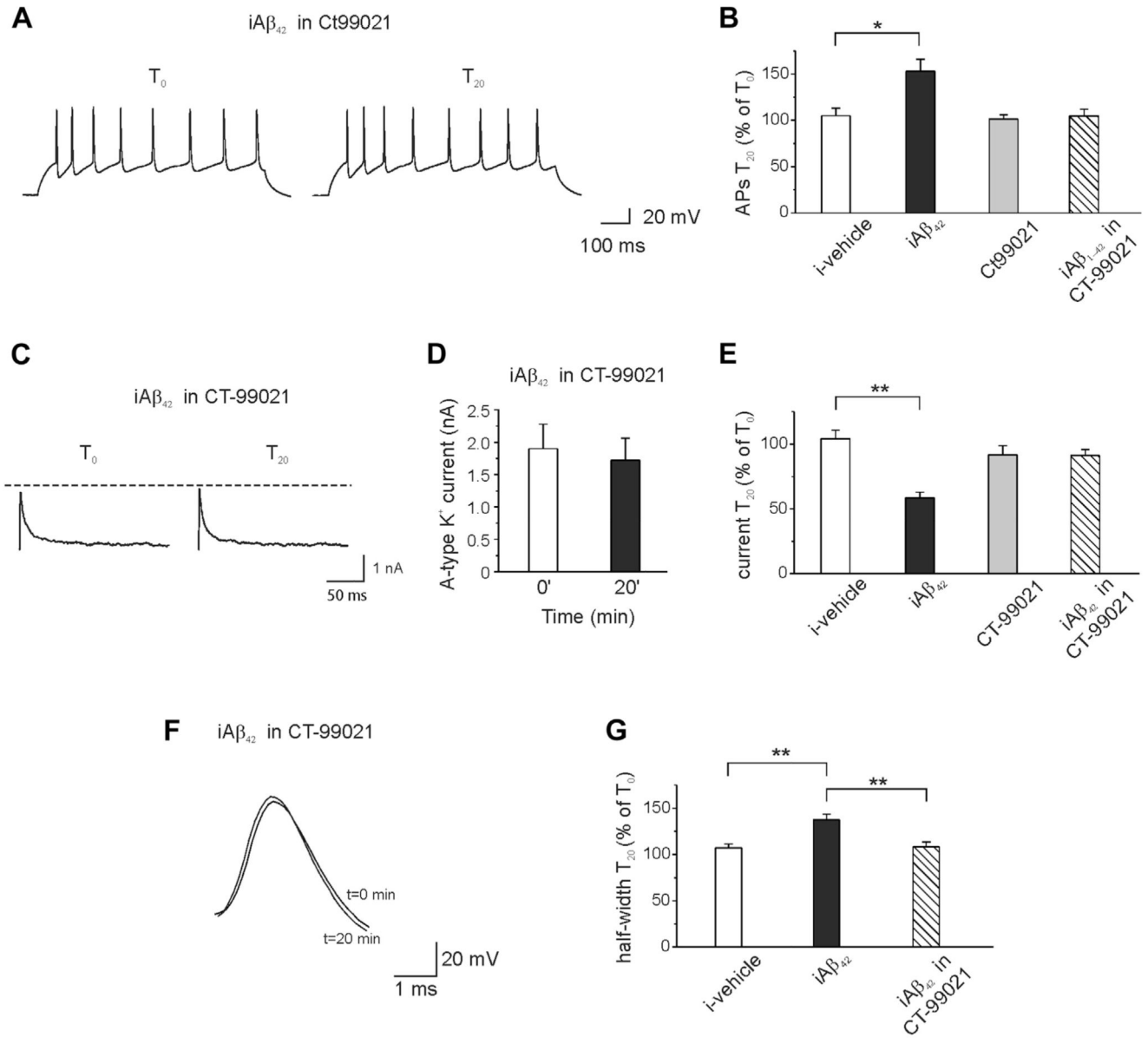

Fig. 4.

Pharmacologic inhibition of GSK-3 prevents iAβ_{42}-induced neuronal hyperexcitability. (A) Representative traces showing that when neurons were preincubated with the GSK-3 inhibitor CT-99021 (1 μM; 20 minutes) intraneuronal application of Aβ_{42} had no effect on spike firing. (B) Bar graph showing percentage of APs number recorded after 20 minutes intracellular perfusion of Aβ_{42} in the presence of CT-99021 (ANOVA test with Tukey post hoc; $F_{(3,37)} = 4.4$; *$p < 0.05$). For comparison, the effect of vehicle and iAβ_{42} are shown (same data of Fig. 1). (C) A-type K^+ currents were unaffected by iAβ_{42} when neurons were preincubated with CT-99021. (D) Bar graph showing the mean current amplitudes in the 2 different conditions (n = 7). (E) Bar graph summarizing data for transient A-type K^+ current experiments (ANOVA test with Tukey post hoc; $F_{(3,32)} = 14.2$; **$p < 0.001$). (F) Preincubation of neurons with CT-99021 prevented the iAβ_{42}-induced increase in the spike

broadening (n = 11). (G) Bar graph summarizing data from experiments shown in F (ANOVA test with Tukey post hoc; $F_{(2,29)} = 11.5$; $^{**}p < 0.001$). Abbreviations: Aβ, amyloid β-protein; ANOVA, analysis of variance; APs, action potentials; iAβ, intracellular Aβ.

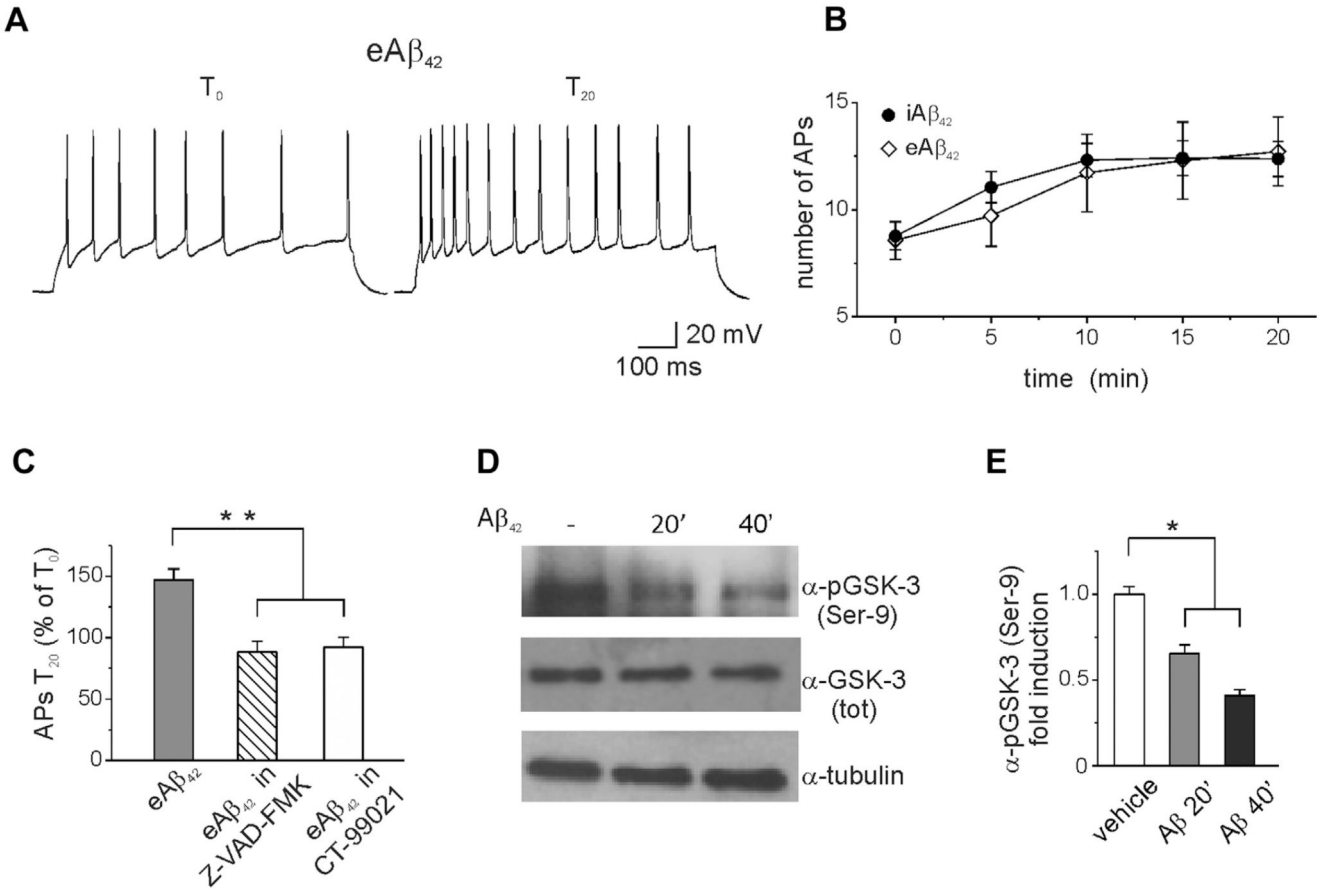

Fig. 5.

Extracellular applied $A\beta_{42}$ increases neuronal excitability to the same extent of $iA\beta_{42}$. (A) Representative traces showing the increase in spike numbers after 20 minutes of extracellular application of $A\beta_{42}$ (200 nM). (B) Time course of increased excitability during extracellular application of $A\beta_{42}$ (n = 7). For comparison, the time course of $iA\beta_{42}$ is also shown (same data of Fig. 1). (C) Bar graph summarizing the effect of $eA\beta_{42}$ on spike discharge. Note that preincubation of neurons with either Z-VAD-FMK (1 μM) or CT-99021 (1 μM) prevented the $eA\beta_{42}$-induced increase in excitability (ANOVA test with Tukey post hoc; $F_{(2,20)} = 17.2$; $^{**}p < 0.001$). (D) Representative Western blots of hippocampal proteins showing decreased immunoreactivity for phosphorylated GSK-3 at Ser-9 following 20–40 minutes of $A\beta_{42}$ treatment. (E) Densitometry for the blots probed with Ser-9 phosphorylated GSK-3 normalized to total GSK-3 is shown (n = 3; $^{*}p < 0.05$; statistics by Mann-Whitney test). Abbreviations: Aβ, amyloid β-protein; ANOVA, analysis of variance; eAβ, extracellular Aβ; iAβ, intracellular Aβ.

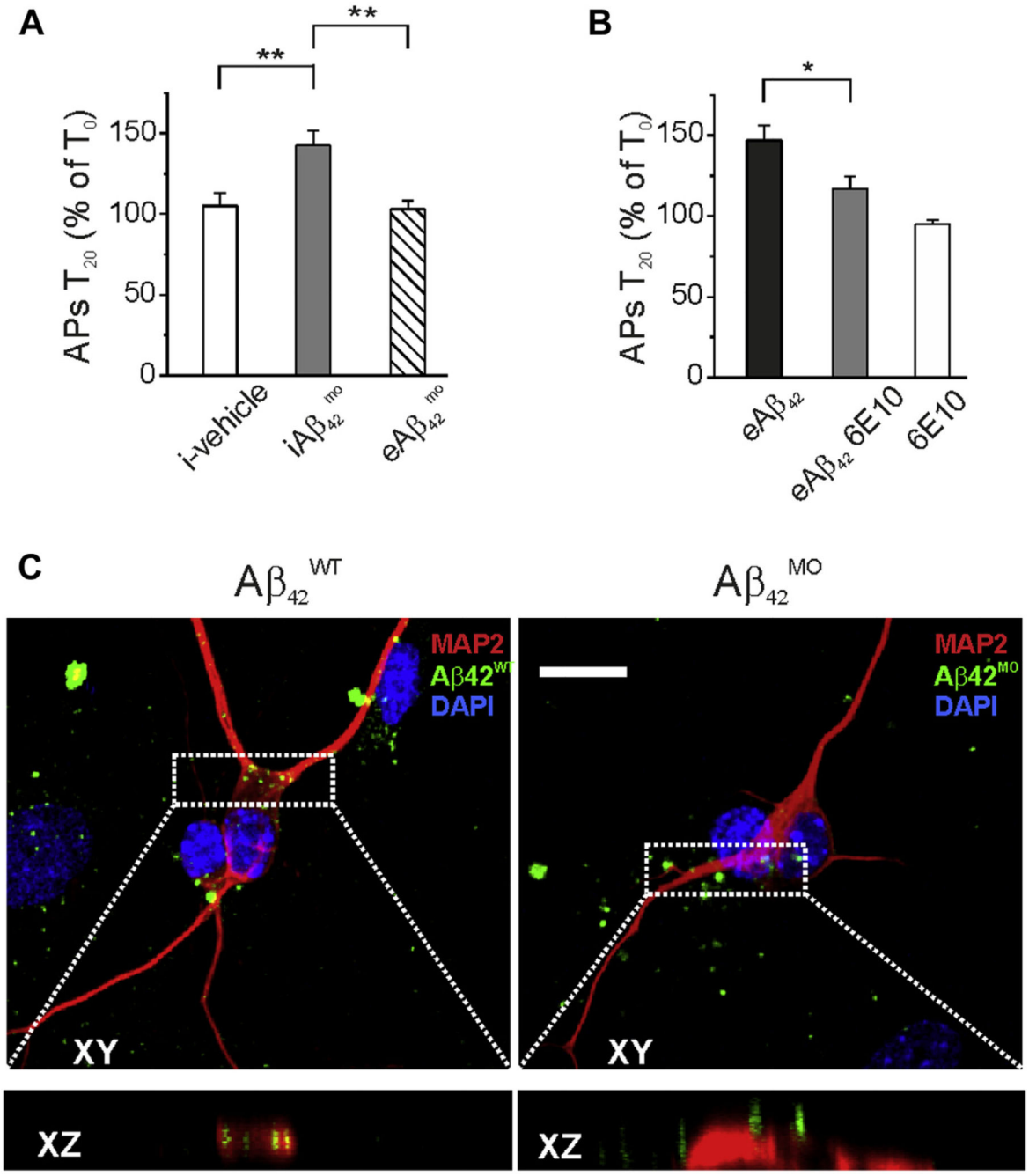

Fig. 6.

Extracellular Aβ$_{42}$-induced hyperexcitability requires neuronal internalization. (A) Summary graphs showing that $A\beta_{42}^{MO}$ increases neuronal excitability only if applied intracellularly (ANOVA test with Tukey post hoc; $F_{(2,20)} = 9.8$; $^{**}p < 0.001$). (B) Bar graph showing that intracellular perfusion of 6E10 by patch pipette significantly reduced the effect of extracellular Aβ$_{42}$ perfusion on neuronal excitability (n = 10; * $p < 0.05$). (C) Representative examples of neurons following 20 minutes extracellular application of 200 nM IRIS-labeled Aβ$_{42}$ (green; left) and $A\beta_{42}^{MO}$ (green; right). Red staining indicates MAP2

immunoreactivity. Scale bar 10 μm. Bottom boxes represent XZ cross-sections from confocal Z-stacks showing the different neuronal accumulation of $A\beta_{42}$ analogues after 20-minute treatments. Abbreviations: Aβ, amyloid β-protein; ANOVA, analysis of variance; MAP2, microtubule-associated protein 2. (For interpretation of the references to color in this Figure, the reader is referred to the Web version of this article.)

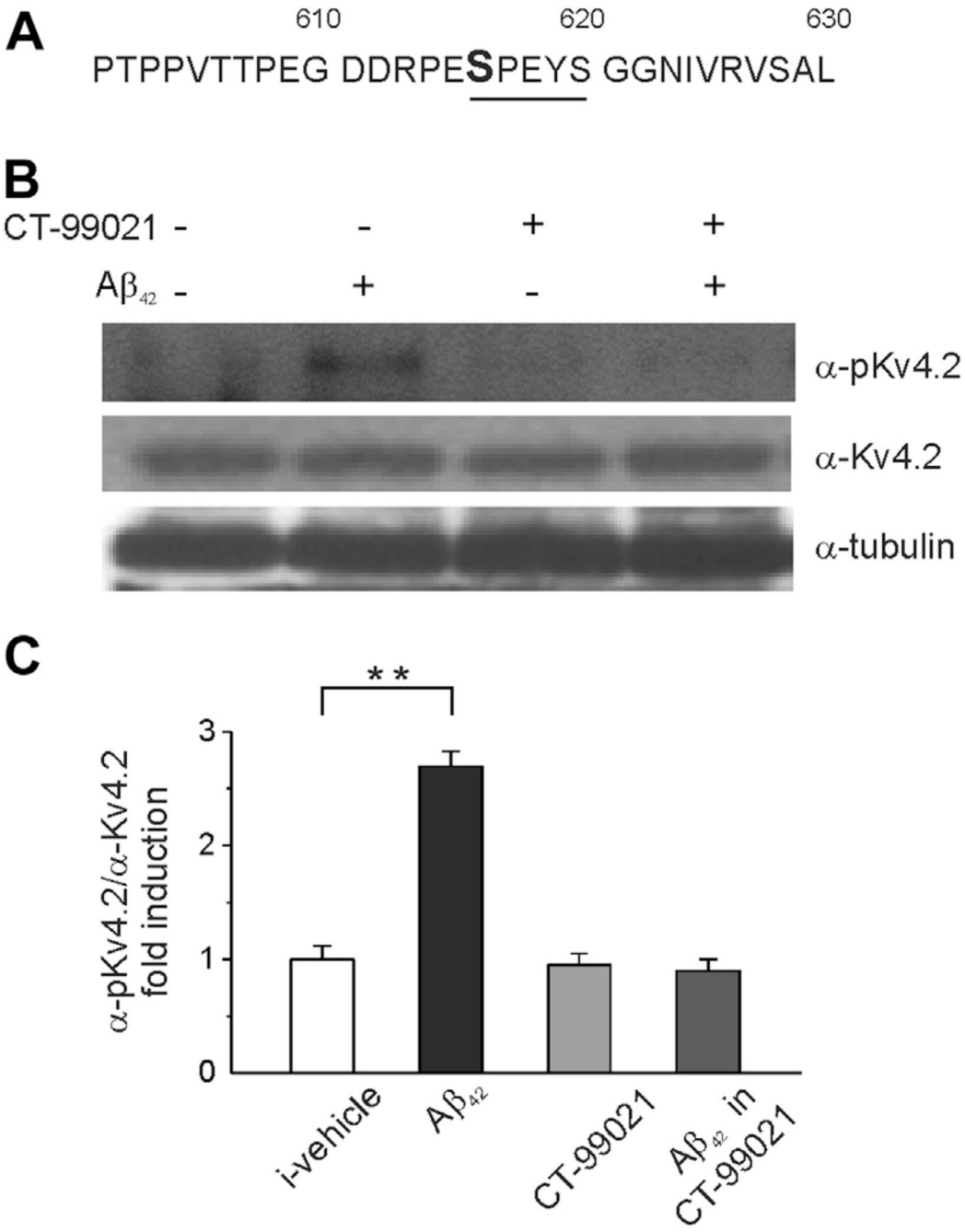

Fig. 7.

$A\beta_{42}$ accumulation leads to GSK-3-dependent phosphorylation of Kv4.2 channel. (A) Primary sequence of the C-terminal domain of Kv4.2 channels around the putative GSK-3 phosphorylation site Ser-616. (B) Representative blots of total cell lysate from primary hippocampal neurons probed with either anti-phospho-Ser-616 (upper panel) or total Kv4.2 (lower panel) antibody following 20 minutes exposure of 200 nM of $A\beta_{42}$ in the presence or absence of CT-99021 (1 μM; 30 minutes). (C) Densitometry analysis for the blots probed

with the anti-phospho-Ser-616 and normalized to total Kv 4.2 channel is shown (n = 3; $^{**}p < 0.001$; statistics by Mann-Whitney test). Abbreviation: Aβ, amyloid β-protein.

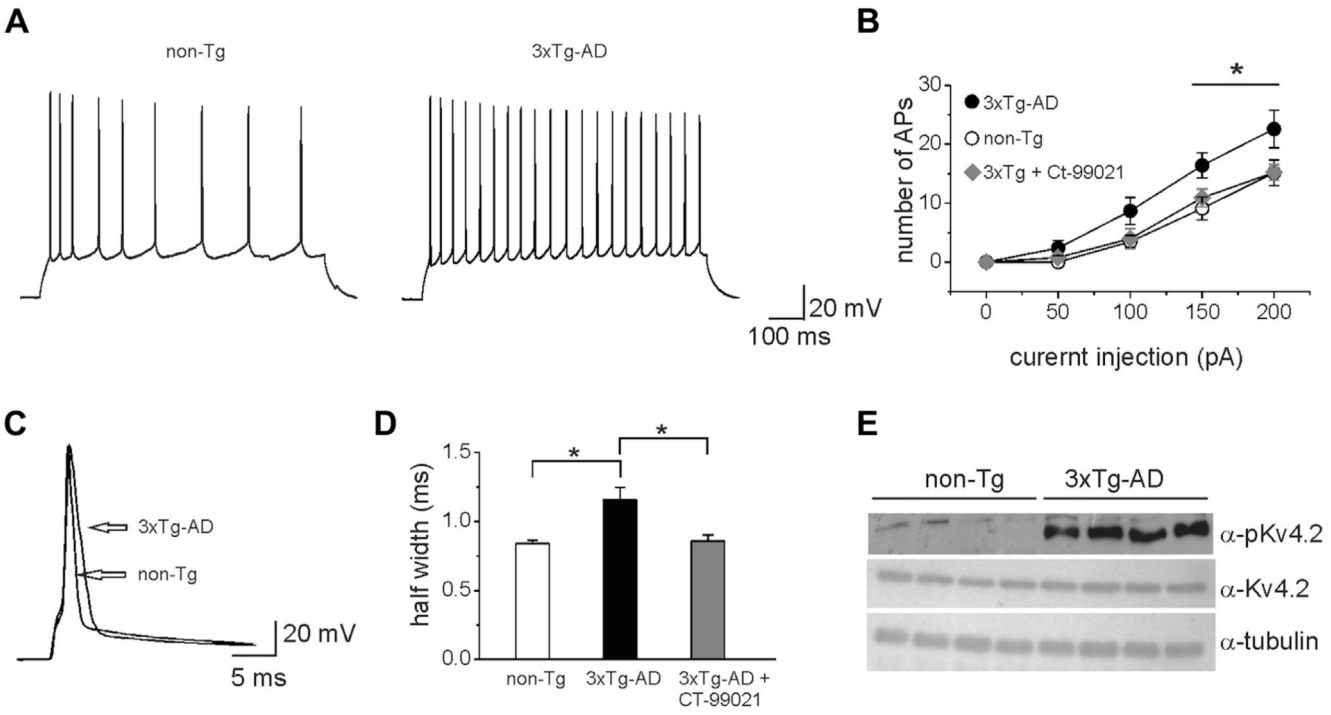

Fig. 8.

CA1 hippocampal pyramidal neurons from 3xTg-AD mouse show increased intrinsic excitability and Kv4.2 channel phosphorylation. (A) Representative current-clamp traces from CA1 hippocampal pyramidal neurons of either 3xTg-AD or non-Tg mice showing AP trains in response to current injection of 150 pA. (B) Input-output curves of APs number versus injected current intensity recorded in slices from 3xTg-AD and non-Tg mice. Note that in 3xTg-AD slices preincubated with CT-99021, the APs number was similar to what was observed in non-Tg mice ($p < 0.05$, unpaired t test; n = 10). (C) Representative AP traces to illustrate AP width in response to a single step current injection (1 nA; 1 ms) in either 3xTg-AD or non-Tg neurons. (D) Bar graph summarizing the mean AP half width in the different experimental groups (n = 10). (E) Representative Western blots of total cell lysate showing increased immunoreactivity for Ser-616 phosphorylation of Kv4.2 in the 3xTg-AD mice compared with non-Tg mice. Note that the total Kv4.2 pool was unchanged in the 2 experimental groups. Abbreviations: 3xTg-AD, triple-transgenic mouse model of Alzheimer's disease; AP, action potential; non Tg, non transgenic.